iScience

CellPress
OPEN ACCESS

Article

Human Herpesvirus 6B Greatly Increases Risk of Depression by Activating Hypothalamic-Pituitary -Adrenal Axis during Latent Phase of Infection

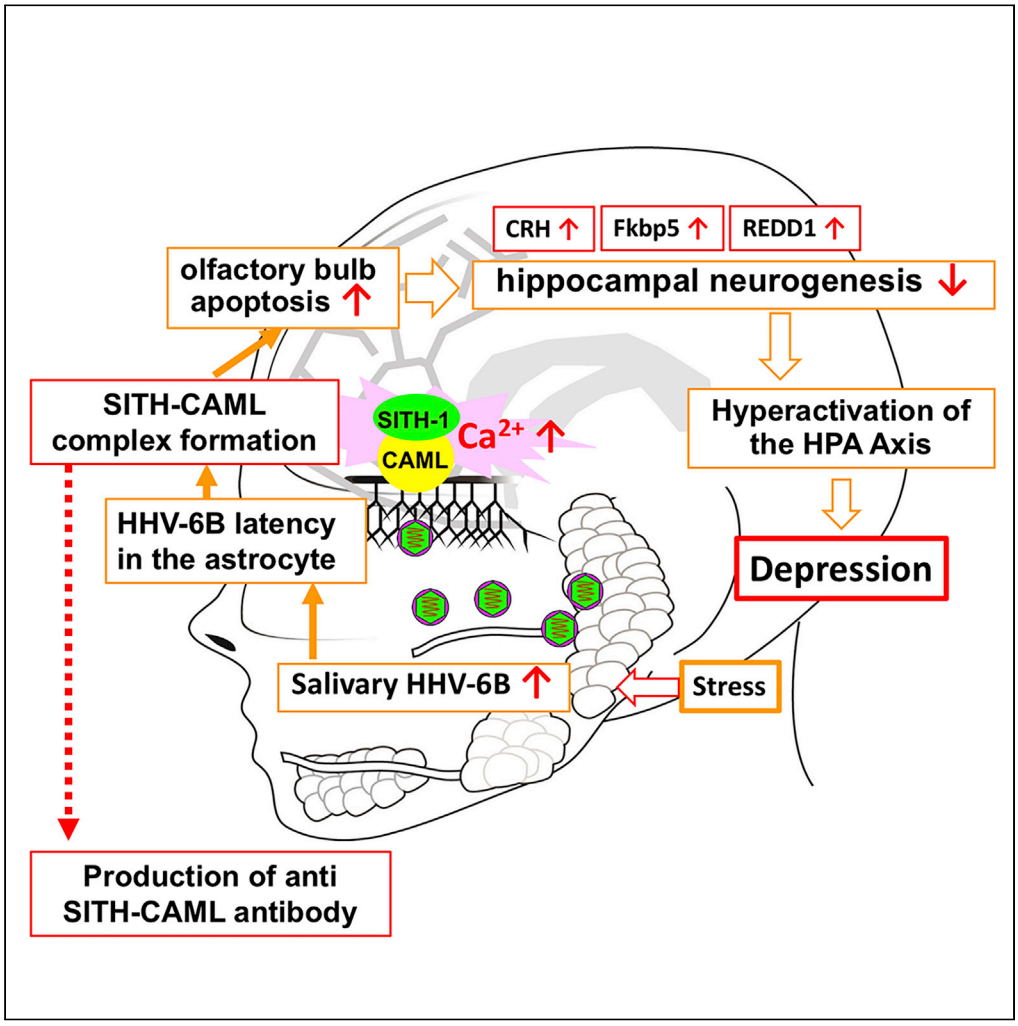

Nobuyuki Kobayashi, Naomi Oka, Mayumi Takahashi, ..., Masahiro Shigeta, Hiroyuki Yanagisawa, Kazuhiro Kondo

kkondo@jikei.ac.jp

HIGHLIGHTS

We identified SITH-1, a new protein specific to HHV-6B latent infection

Mice expressing SITH-1 at HHV-6B latent infection site had depressive symptoms

Depressive symptoms due to SITH-1 were associated with a hyper-activated HPA axis

SITH-1-specific antibody detection significantly greater in depressive patients

Kobayashi et al., iScience *23*, 101187
June 26, 2020
https://doi.org/10.1016/j.isci.2020.101187

iScience

CellPress
OPEN ACCESS

Article

Human Herpesvirus 6B Greatly Increases Risk of Depression by Activating Hypothalamic-Pituitary -Adrenal Axis during Latent Phase of Infection

Nobuyuki Kobayashi,[1,2,5] Naomi Oka,[1,5] Mayumi Takahashi,[1] Kazuya Shimada,[1] Azusa Ishii,[1] Yoshitaka Tatebayashi,[3] Masahiro Shigeta,[2] Hiroyuki Yanagisawa,[4] and Kazuhiro Kondo[1,6,*]

SUMMARY

Little is known about the effect of latent-phase herpesviruses on their host. Human herpesvirus 6B (HHV-6B) is one of the most ubiquitous herpesviruses, and olfactory astrocytes are one of the most important sites of its latency. Here, we identified SITH-1, an HHV-6B latent protein specifically expressed in astrocytes. Mice induced to produce SITH-1 in their olfactory astrocytes exhibited olfactory bulb apoptosis, a hyper-activated hypothalamic-pituitary-adrenal (HPA) axis and depressive symptoms. The binding of SITH-1 to the host protein calcium-modulating ligand (CAML) to form an activated complex promoted the influx of extracellular calcium. The serum antibody titers for depressive patients with respect to this activated complex were significantly higher than for normal controls ($p = 1.78 \times 10^{-15}$), when the antibody positive rates were 79.8% and 24.4%, respectively, and the odds ratio was 12.2. These results suggest that, in the latent phase, HHV-6B may be involved in the onset of depression.

INTRODUCTION

Herpesviruses have the property to maintain a state of latent infection in hosts throughout their lives and are an important component of the viral microbiome (virome), which occasionally increases the risk of various diseases (Virgin and Todd, 2011; Virgin et al., 2009).

Human herpesvirus 6B is a ubiquitous, neurotrophic virus that is widespread in many parts of the world, including the USA, Europe, and Japan. It causes roseola in the initial infection and afterward establishes latency. The virus is reactivated in response to immunosuppression in transplant patients and sometimes causes encephalitis (Ablashi et al., 2014).

Recent postmortem research revealed that HHV-6B and HHV-6A, a close relative of HHV-6B, had been reactivated from the latent state and had caused productive infection in the cerebellum in patients with mood disorders (major depressive disorder and bipolar disorder [BPD]) (Prusty et al., 2018). Although many aspects of the relationship between HHV-6A/B and these diseases were unknown, the authors stated the importance of conducting research on the mechanism by which latent HHV-6A/B are reactivated and infect the brain. Other past research reported detection of HHV-6B DNA in the orbital frontal cortex of patients with BPD (Conejero-Goldberg et al., 2003).

Proposed sites of HHV-6B latency are the tonsils and adenoids, and the virus has been shown to be actively shed in saliva. The shed virus enters the olfactory pathway and establishes latency in the astrocytes in the olfactory bulb/tract and nasal endothelium, other sites of HHV-6B latency (Ablashi et al., 2014; Donati et al., 2005; Harberts et al., 2011).

The olfactory bulb (OB) is not only a site of HHV-6B latency but also an immune organ that prevents virus in the saliva from invading the brain (Durrant et al., 2016). So, it is possible that the state of the OB is strongly associated with the reactivation of HHV-6B and invasion into the brain. OB dysfunction and a decrease in its volume have been reported in depressive patients (Negoias et al., 2010; Rottstaedt et al., 2018). We therefore considered that the effect of HHV-6B infection on the OB and other parts the olfactory system would differ between depressive patients and normal controls (NCs). As it has been reported that HHV-6B

[1]Department of Virology, The Jikei University School of Medicine, 3-25-8 Nishi-Shimbashi, Minato-ku, Tokyo 105-8461, Japan

[2]Department of Psychiatry, The Jikei University School of Medicine, 3-25-8 Nishi-Shimbashi, Minato-ku, Tokyo 105-8461, Japan

[3]Affective Disorders Research Team, Tokyo Metropolitan Institute of Medical Science, 2-1-6 Kamikitazawa, Setagaya-ku, Tokyo 156-8506, Japan

[4]Department of Public Health & Environmental Medicine, The Jikei University School of Medicine, 3-25-8 Nishi-Shimbashi, Minato-ku, Tokyo 105-8461, Japan

[5]These authors contributed equally

[6]Lead Contact

*Correspondence: kkondo@jikei.ac.jp

https://doi.org/10.1016/j.isci.2020.101187

infection in olfactory tissues is mainly latent infection (Harberts et al., 2011), our aim was to study the effects of latent infection.

However, the effects of herpesviruses in the latent state on the host have been clarified in only a few cases, examples of which are oncogenetic herpesviruses, such as Epstein-Barr virus and Kaposi's sarcoma-associated herpesvirus. As reasons that the effects of these viruses are clearly known: first, the proteins produced by them during latency (latent proteins) have been identified; second, the functions of their latent proteins are well understood (Jha et al., 2016). Therefore, we thought that analysis of latent proteins produced by HHV-6B might clarify its effects on the host during latency. Astrocytes are considered to be the cells in the olfactory system latently infected by HHV-6B (Donati et al., 2005; Harberts et al., 2011), so we first attempted to identify a latent protein produced by HHV-6B in astrocytes during latency.

RESULTS

Identification of SITH-1, a New HHV-6B Latent Infection Protein

In order to identify astrocyte-specific HHV-6B latent protein, we used the latent protein of human cytomegalovirus (HCMV), a close relative of HHV-6B, as a reference. In our previous research, we identified two cytomegalovirus latent transcripts (CLTs) that code for latent proteins in HCMV. One of these CLTs (CLT ORF94) codes for latent protein open reading frame (ORF) 94, which consists of 94 amino acids, and the other (CLT ORF152) for ORF152, consisting of 152 amino acids (Kondo et al., 1996). In HHV-6B, we had already identified HHV-6 latent transcript (H6LT) type I and H6LT type II, homologs of CLT ORF94. They are expressed in macrophages and have the capacity to regulate reactivation of HHV-6B (Kondo et al., 1991, 2003), which suggests that they are related to HHV-6B latency in tonsils and adenoids.

In the present research, we looked for a homolog of CLT ORF152. This led to identifying a new HHV-6B latent transcript that codes for a protein consisting of 159 amino acids, and we named it Small protein encoded by the Intermediate stage Transcript of HHV-6-1 (SITH-1) (Figures 1A and S1A–S1D). This protein had amino acid homology (20% identity, 74% similarity) with ORF152 (Kondo et al., 1996). We studied SITH-1 expression using macrophage (MΦ) cell lines (THP-1 and HL-60) and astrocyte cell lines (U373 and A172). Although no HHV-6B replication was observed (data not shown) in these cell lines, expression of latency-associated genes U94 (Rotola et al., 1998) and/or H6LT was detected (Figures S1E and S1F) so we considered them to be latency-like gene expressing cells. SITH-1 mRNA was mainly expressed in astrocyte cell lines (U373 and A172) (Figure 1B). Also, SITH-1 protein was produced in HHV-6B-infected U373 cells without production of late proteins (glycoprotein [g]B and gH) (Figure 1C). Based on these properties, SITH-1 was considered to be the latent protein produced during HHV-6B latency in olfactory astrocytes that we were looking for in this study.

Characterization of SITH-1 Expressing Mice

We examined the effects of SITH-1 expression in olfactory astrocytes in mice. We created the mouse model (SITH-1 mouse) through intranasal inoculation with an adenovirus vector (SITH-Ad) possessing the SITH-1 open reading frame (ORF) downstream of the glial fibrillary acidic protein (GFAP) promoter, which is specifically expressed in astrocytes. In the SITH-1 mouse, SITH-1 was produced in olfactory ensheathing cells (OECs), a type of olfactory astrocyte (Figure S2A), and apoptosis occurred in the olfactory bulb (Figures 1D–1F). The apoptosis in the olfactory bulb occurred mainly in astrocytes (Figures S2B–S2D). As impairment of the olfactory bulb has been reported to be associated with depression (Morales-Medina et al., 2017; Rottstaedt et al., 2018), we subjected SITH-1 mice to the tail suspension test (TST) to see if they exhibited depressive symptoms. There was an increase in immobility time, indicating depression-like behavior, which was suppressed by an anti-depressant (SSRI) (Figure 1G). This suggests that the SITH-1 mice were presenting depressive symptoms.

We next studied the SITH-1 mice to see if they manifested the pathological state associated with depression. Since it has been found that depression is induced by stress (Belmaker and Agam, 2008; Keller et al., 2017), we examined an association between SITH-1 mouse behavior and stress. When the mice were subjected to mild stress by tilting their cages, they exhibited decreased sucrose preference, a symptom of depression (Figure 2A). Moreover, the expressions of corticotropin-releasing hormone (CRH) (Keller et al., 2017) and FK506 binding protein 5 (FKBP5) (Scharf et al., 2011) were increased, indicating that the hypothalamic-pituitary-adrenal (HPA) axis, the major component of the stress response, was enhanced (Figures 2B and 2C). Expression of Regulated in development and DNA damage response 1 (REDD1)

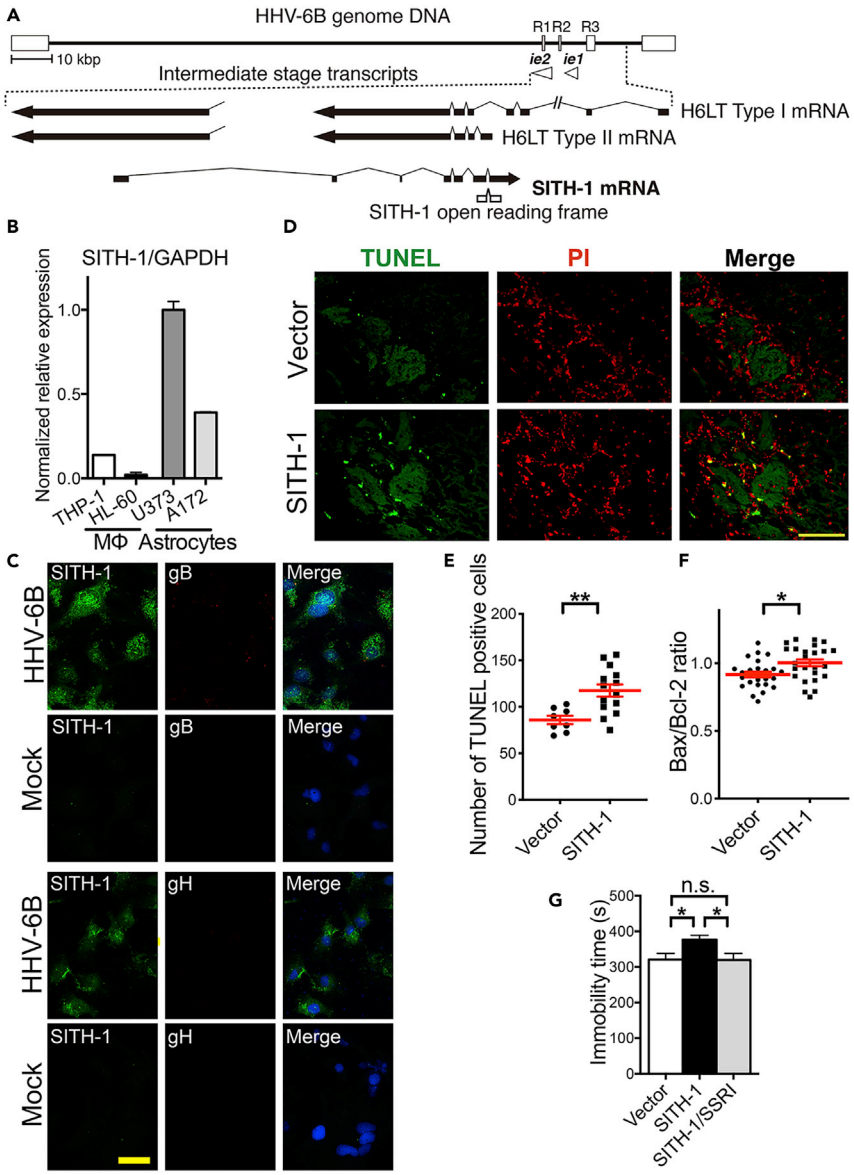

Figure 1. Identification and Characterization of SITH-1

(A) Structures of HHV-6B DNA, H6LT, and SITH-1 mRNA. R1, R2, and R3 indicate repeat regions.

(B) SITH-1 mRNA expression in macrophage (MΦ) cell lines (THP-1 and HL-60) and astrocyte cell lines (U373 and A172). Ratios of SITH-1 to glyceraldehyde-3-phosphate dehydrogenase (GAPDH) are shown.

(C) SITH-1 protein production in HHV-6B-infected U373 cells. Confocal imaging of HHV-6B infected and mock infected U373 cells. The upper six panels show staining with anti-SITH-1 antibodies and anti-gB antibodies and the lower six panels staining with anti-SITH-1 antibodies and anti-gH antibodies. Green, SITH-1; red, gB or gH; blue, DAPI.

(D) Detection of apoptosis in OB using TUNEL staining. Green, TUNEL; red, propidium iodide (PI).

(E) Numbers of TUNEL-positive apoptotic cells in each section.

(F) Enhancement of OB apoptosis detected by increase in Bax/Bcl-2 ratio

(G) Prolonged immobility in TST. One-way ANOVA with Fisher's post hoc test; *, $p < 0.05$; n.s., not significant.

(E and F) Values are means ± SEM. Unpaired t test; *, $p < 0.05$; **, $p < 0.01$.

Scale bars, 100 μm (C and D).

(Ota et al., 2014), which is considered essential to depression induced by HPA axis activation, was also increased (Figure 2D). Steroidogenic acute regulatory protein (StAR) (Otawa et al., 2007), the rate-limiting factor for corticosteroid production in the adrenal gland, was also up-regulated (Figure 2E).

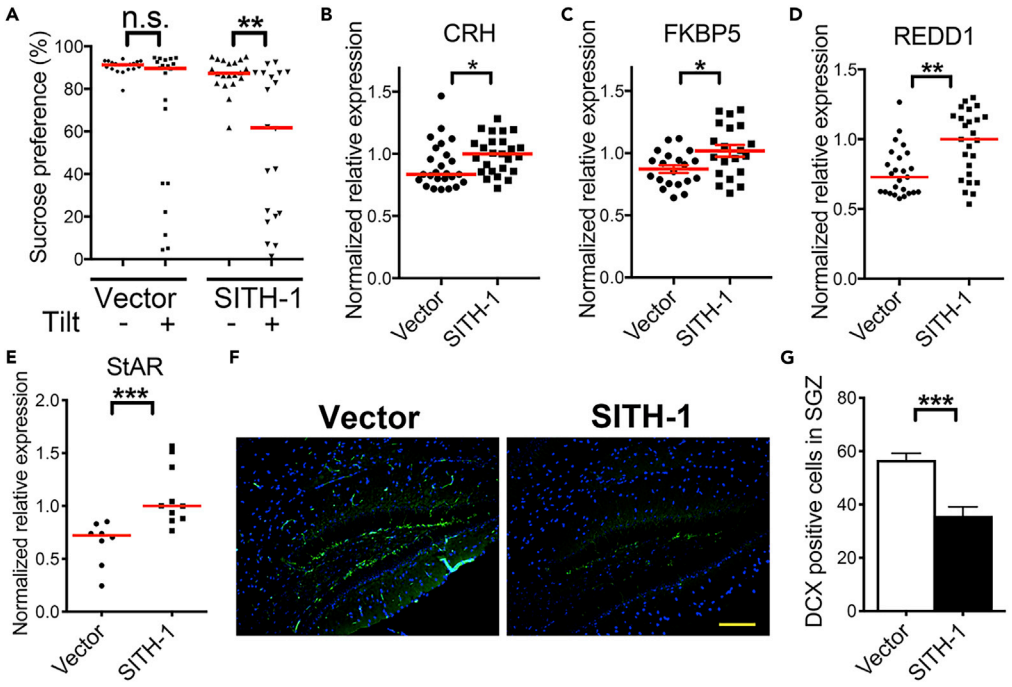

Figure 2. Depression-like Changes in SITH-1 Mice

(A) Enhanced stress in SITH-1 mice. Vector control and SITH-1 mice were caged with (+) or without (–) tilt, and sucrose preference was calculated as % sucrose intake.

(B–E) Up-regulation of indicated mRNAs related to HPA axis activation. (B–D) Up-regulation of indicated mRNAs related to HPA axis activation in the brain. (E) Up-regulation of StAR mRNA in the adrenal gland.

(F) DCX staining of hippocampal dentate gyrus (DG). Green, DCX; blue, DAPI. Scale bar, 100 μm.

(G) Numbers of DCX-positive cells in subgranular zone (SGZ) in each section. Comparison of vector control and SITH-1 mice. Unpaired t test; ***, $p < 0.001$.

(A, B, D, and E) Bars represent median values; Mann-Whitney U-test. *, $p < 0.05$; **, $p < 0.01$; ***, $p < 0.001$; n.s., not significant. (C) Values are means ± SEM. Unpaired t test; *, $p < 0.05$.

A decrease in hippocampal neurogenesis has been reported to be a cause of HPA axis activation in depression (Snyder et al., 2011). Through staining with doublecortin (DCX), a marker of immature neurons, we found that DCX-positive cells in the hippocampus of the SITH-1 mice were decreased (Figures 2F and 2G), indicating a decrease in hippocampal neurogenesis. In subsequent experiments using bromodeoxyuridine (BrdU)-positive cells or DCX and BrdU double-positive cells, similar decreases in neurogeneration were observed (Figures S2E–S2H). Also, it has been reported that hippocampus neurogeneration was decreased in a model of depression in which olfactory bulb function was impaired by bulbectomy (Morales-Medina et al., 2017). Considering these observations together, we believe that SITH-1 suppresses hippocampus neurogeneration via olfactory bulb impairment and, by doing so, activates the HPA axis, which results in the development of depressive symptoms. At this time, as there was no enhancement of inflammatory cytokine expression in the brain or olfactory bulb of the SITH-1 mice, the phenomena observed were considered not to be due to an immune response to SITH-1 (Figures S3A–S3J). Also, to exclude the possibility that SITH-1 expression outside the olfactory system causes depression-like phenomena, we administered SITH-Ad at the same titer as for intranasal inoculation orally and intraperitoneally and examined behavior as well as gene expression. No depression-like behavior or increase in depression-related gene expression was observed (Figures S4 and S5).

Functional Analysis of SITH-1

Next, we examined the mechanism by which SITH-1 induced apoptosis in astrocytes of the olfactory bulb. In two-hybrid screening, human calcium-modulating cyclophilin ligand (CAML) was identified as a protein binding to SITH-1 (data not shown). The binding of SITH-1 and CAML was suggested by the mammalian two-hybrid system (Figure 3A). CAML has been found to promote the influx of calcium into cells (Holloway and Bram, 1996). Also, it is believed to manifest this function through binding with other molecules in cells (Yamamoto and Sakisaka,

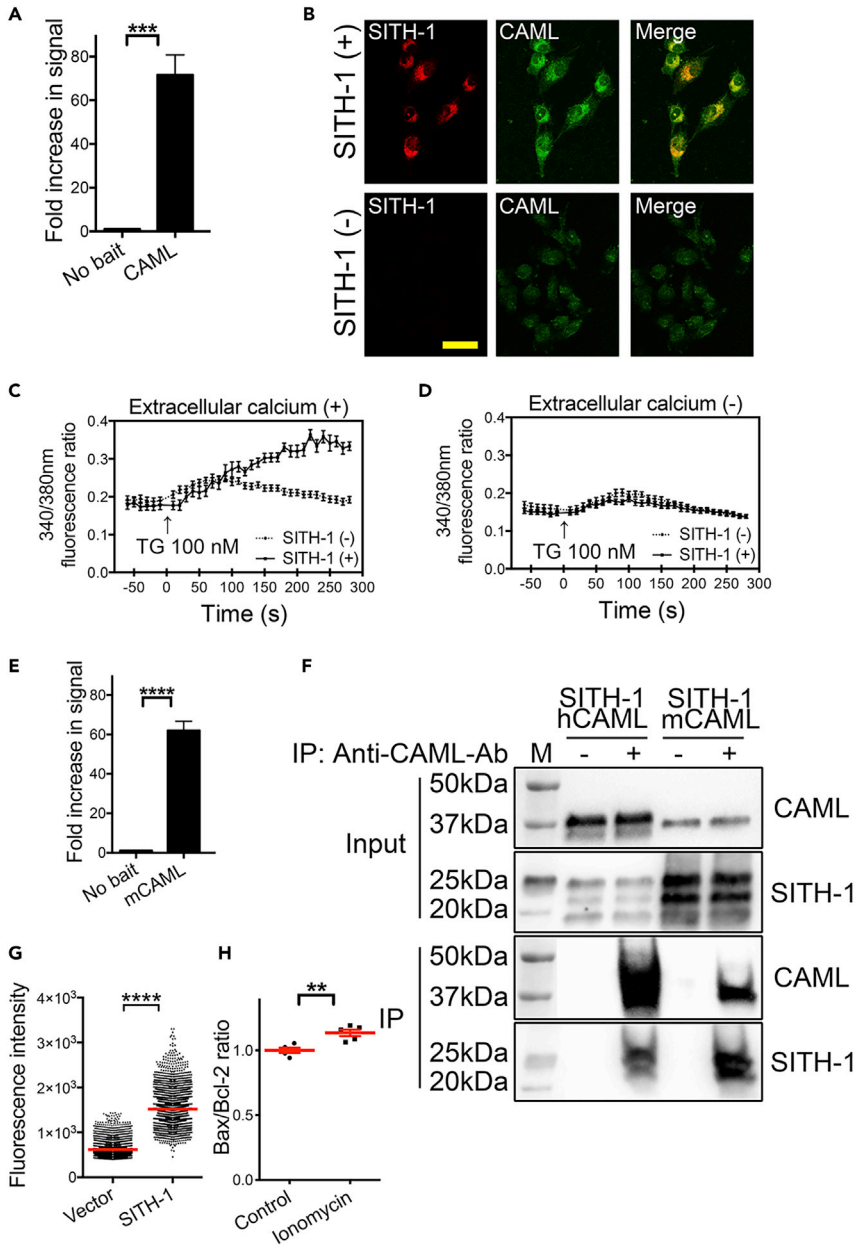

Figure 3. Characterization of SITH-1

(A) Binding activity of SITH-1 and CAML.

(B) Colocalization of SITH-1 and CAML in astrocytes. U373 cells expressing SITH-1 (SITH-1[+]) and not expressing SITH-1 (SITH-1[−]) were immunostained. Confocal images are shown. Red, SITH-1; green, CAML. Scale bar, 100 μm.

(C and D) Promotion of intracellular calcium influx by SITH-CAML complex with extracellular calcium (C) and without it (D). U373 cells expressing (SITH-1[+]) or not expressing SITH-1(SITH-1[−]) were stimulated with thapsigargin (TG) at time 0. Values are means ± SEM.

(E) Binding activity of SITH-1 and mCAML determined by a mammalian two-hybrid assay.

(F) Co-immunoprecipitation assay in cells co-expressing SITH-1 and CAML. After immunoprecipitation using anti-CAML antibodies, western blot analyses were performed using anti-CAML antibodies and anti-SITH-1 antibodies. The upper two panels show input cell lysate and the lower two panels show immunoprecipitated samples. hCAML, human CAML; mCAML, mouse CAML; M, molecular weight marker.

(G) Increased calcium concentration in mouse 3T3 cells due to SITH-1 expression. Bars represent median values; Mann-Whitney U-test. ****, $p < 0.0001$.

Figure 3. *Continued*
(H) Enhancement of OB apoptosis by calcium ionophore.
(A, E, and H) Unpaired t test; **, $p < 0.01$; ***, $p < 0.001$; ****, $p < 0.0001$. Values are means ± SEM (H).

2015). When SITH-1 was expressed in the human U373 astrocyte cell line, using confocal fluorescence microscopy, we observed the colocalization of SITH-1 and CAML as well as an increase in immunofluorescence intensity, suggesting accumulation of the SITH-CAML complex (Figures 3B and S6). In addition, in the U373 cells in which SITH-1 was expressed, in the presence of extracellular calcium, there was an increase in intracellular calcium concentration (Figures 3C and 3D). In view of this, the complex of SITH-1 and CAML was considered to have the property to induce influx of extracellular calcium into cells. Human CAML and mouse CAML (mCAML) have high homology (88% identity, 98% similarity), and the binding of SITH-1 and mCAML was suggested by the mammalian two-hybrid system (Figure 3E). For further confirmation of the binding of SITH-1 and CAML determined using the mammalian two-hybrid system, we carried out a co-immunoprecipitation assay. Into HEK293T cells, which have hardly any endogenous CAML production, we transfected SITH-1 as well human or mouse CAML and carried out immunoprecipitation using anti-CAML antibodies. SITH-1 and CAML were co-immunoprecipitated, clearly showing that SITH-1 bound with both human and mouse CAML (Figure 3F). In addition, SITH-1 brought about an increase in intracellular calcium concentration in mouse cells (Figure 3G).

In order to confirm whether influx of extracellular calcium induced apoptosis in the olfactory bulb, we administered a calcium ionophore with a Ca^{2+} transport enhancing action in the cell membrane into the nasal cavity of the mice. This resulted in enhancing apoptosis in the olfactory bulb (Figure 3H). An increase in calcium concentration in OECs has caused ectopic neurovascular coupling in the olfactory bulb via release of ATP and glutamate (Thyssen et al., 2010), and by causing cerebrovascular stenosis (Mulligan and MacVicar, 2004) it could be associated with olfactory bulb cell impairment. In view of this, we consider that the mechanism by which SITH-1 induces apoptosis in the olfactory bulb is based on the promotion of extracellular calcium influx into OECs by the complex of SITH-1 and CAML.

Evidence for SITH-1 Expression in Depressive Patients

Next, we developed a method for investigating whether calcium influx due to SITH-1 occurs *in vivo* in depressive patients. Owing to the high invasiveness and difficulty of directly detecting SITH-1 expressed in the olfactory system, we decided to investigate the production of antibodies to the complex of SITH-1 and CAML. Based on a study using the SOSUI secondary structure prediction system (Hirokawa et al., 1998), the complex was assumed to be one with SITH-1 at the N terminus and CAML at the C terminus (N-SITH-CAML-C) (Figures S7A–S7D). We measured intracellular calcium concentrations for cells expressing each of the structures shown in Figures S7A–S7D. As we had expected, N-SITH-CAML-C was strongest in promoting calcium influx, whereas a complex with CAML at the N terminus and SITH-1 at the C terminus (N-CAML-SITH-C) achieved hardly any calcium influx (Figure 4A). Also, the strongest serum antibody reaction in the SITH-1 mice was with respect to N-SITH-CAML-C (Figures 4B and 4C). Based on these observations, the antibodies produced *in vivo* in the SITH-1 mice to the SITH-1-CAML complex were anti-N-SITH-CAML-C antibodies. Thus, through measurement of these antibodies, it should be possible to study the formation of the SITH-CAML complex and calcium influx *in vivo*.

We next measured anti-N-SITH-CAML-C antibodies in depressive patients. Similar to the SITH-1 mouse, the serum antibody reaction in depressive patients was strongest with respect to N-SITH-CAML-C (Figures 4D and 4E). Also compared with normal controls, the anti-N-SITH-CAML-C antibody titer was higher in depressive patients ($p = 1.78 \times 10^{-15}$) (Figure 4F). In analysis using receiver operating characteristic (ROC) curves, the area under the curve (AUC) was 0.8573, the antibody positive rates were 79.8% for depressive patients and 24.4% for healthy subjects, and the odds ratio was 12.2 (cutoff value 1.957) The use of Anti-N-SITH-CAML-C antibodies achieved diagnostic accuracy of 77.7% for depression (Figure S7E). There was no difference between depressive patients and normal controls (NCs) regarding antibody titers for HHV-6 (Figure S7F). Based on these findings, we considered that more SITH-CAML complex was being formed in depressive patients and that calcium influx was enhanced. Compared with NCs who had no depressive symptoms (Beck Depression Inventory [BDI] ≤ 3), the anti-N-SITH-CAML-C antibody titer was higher in NCs who had a few depressive symptoms ($4 \leq$ BDI ≤ 10) (Figure 4G). This finding may support the contribution of SITH-CAML to the risk of depression. There were no significant differences in sex ratio or age between depressive patients and NCs (Table S1).

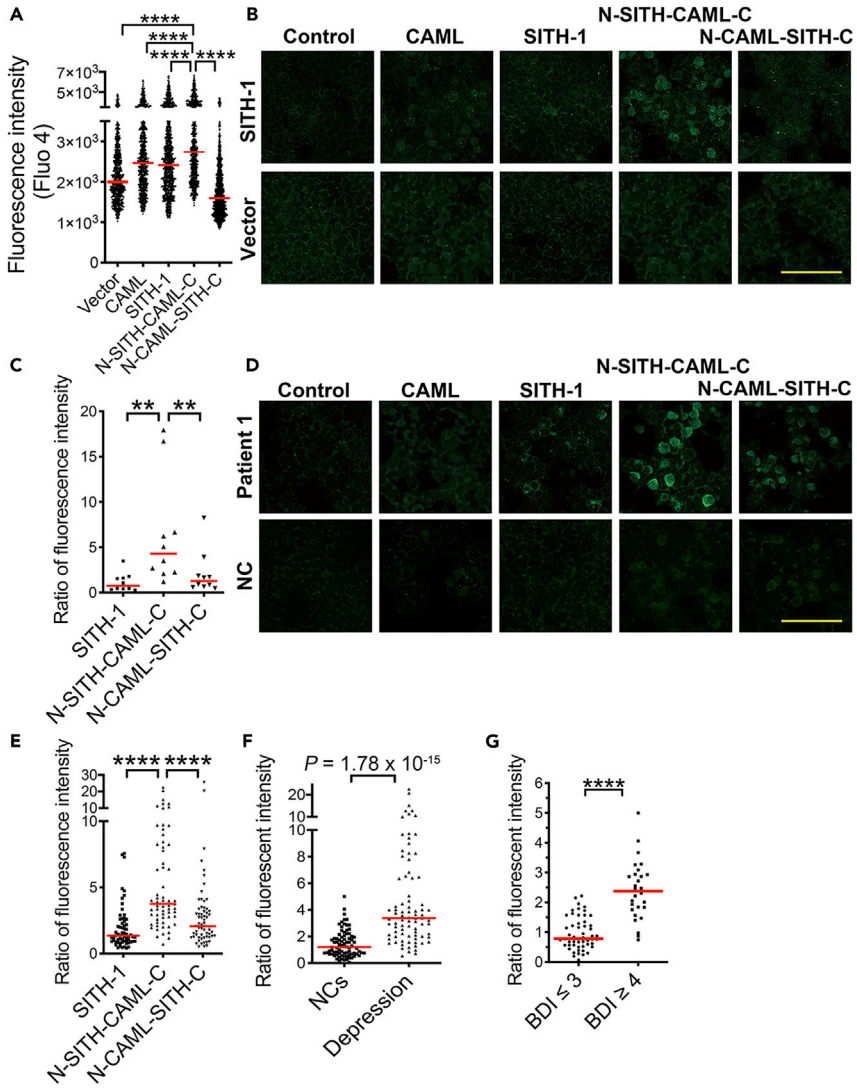

Figure 4. Formation of SITH-CAML Complex in Depressive Patients

(A) Intracellular calcium concentrations in various protein expressing cells.

(B) Antibody response to various antigens in mice. Shows representative IFA images for SITH-1 mice and vector control mice for various antigens. Scale bar, 100 μm.

(C) Comparison of antibody titers for N-SITH-CAML-C, N-CAML-SITH-C and SITH-1in SITH-1 mice.

(D) Antibody reactions to various antigens in depressive patients. Shows representative IFA images for individual antigens in one patient and one normal control (NC). Scale bar, 100 μm.

(E) Comparison of antibody titers for N-SITH-CAML-C, N-CAML-SITH-C, and SITH-1 in depressive patients.

(F) Elevated anti-N-SITH-CAML-C titers in depressive patients.

(G) Comparison of anti-N-SITH-CAML-C antibody titers in normal controls with BDI up to 3 and 4 or greater.

Bars represent median values, and Kruskal-Wallis test with Steel's post hoc test (A, C, and E) and Mann-Whitney U-test (F and G). **, $p < 0.01$; ****, $p < 0.0001$.

DISCUSSION

In the present research, we identified the HHV-6B latent protein SITH-1, and our findings in a mouse model in which SITH-1 was expressed in the olfactory astrocytes suggested that its binding with CAML enhanced calcium influx into cells and promoted OB apoptosis.

We also measured antibodies (anti-N-SITH-CAML-C antibodies) to the SITH-1-CAML complex in human serum. Differing from postmortem examination of brains, detection of antibodies is an indirect method

of evaluation, but it is minimally invasive and has the advantage of applicability as a test in patients who currently have depression. The detection rate of Anti-N-SITH-CAML-C antibodies in depressive patients was 79.8%, with a diagnostic accuracy of 77.7% for depression. In a previous study on antiphospholipid syndrome (APS), antibodies that react with the structure of active form β2-glycoprotein 1 were reported to be important for detection of APS (Pelkmans and de Laat, 2012). In the present study, the structure recognized by the detected antibodies was the SITH-1-CAML complex, which promotes calcium influx into cells, suggesting the possibility that they recognized a disease-related structure as in the case of APS.

Regarding an association with the OB, in imaging diagnosis, a decrease in OB volume was observed in depressive patients and diagnostic accuracy for depression based on this decrease was reported to be 68.1% (Rottstaedt et al., 2018). Thus, the diagnostic accuracy for depression using N-SITH-CAML-C antibodies in the present study and that using OB volume were close to each other, so it is conceivable that OB apoptosis due to SITH-1 expression similar to that in the mouse model occurs in depressive patients.

Using the mouse model, we found that promotion of OB apoptosis by SITH-1 activated the HPA axis. Since activation of the HPA axis has been observed to suppress host immune function by increasing corticosteroid production, its activation is thought to be advantageous for HHV-6B survival and reactivation. In addition, the OB is reportedly an immune organ that prevents viruses from invading the brain (Durrant et al., 2016) and induction of apoptosis in the OB may help HHV-6B in saliva to reach the brain. In this regard, a postmortem study reported proliferation of HHV-6B in cerebellums from depressive patients (Prusty et al., 2018).

We still know little about the cause of depression, and even in large-scale genetic analyses, no genes with an odds ratio of greater than 1.2 for an influence in depression have been discovered (Major Depressive Disorder Working Group of the Psychiatric GWAS Consortium et al., 2013; Levinson et al., 2014). In the results of the present study, at 12.2, the odds ratio for SITH-1-CAML complex antibody positivity having an influence in depression was extremely high. In view of this, multiple factors could be at work in the influence of HHV-6B and SITH-1 in depression.

HPA axis activation is known to raise depression risk (Belmaker and Agam, 2008; Keller et al., 2017). Also, the immunosuppression due to a hyper-activated HPA axis and decreased immune function caused by OB impairment would promote HHV-6B proliferation in the brain as suggested above. In addition, risks for depression have been reported for pathogens apart from HHV-6B, which include other herpesviruses and chlamydia (Wang et al., 2014). HPA axis activation and OB impairment may increase the risk of depression by facilitating the infiltration of these pathogens into the brain and their subsequent proliferation.

The mechanism by which SITH-CAML complex is produced in greater quantities in depressive patients than in normal controls will need to be studied further in the future. As a possibility, overwork is known to increase salivary HHV-6B (Aoki et al., 2016), and in this case, the increase in HHV-6B could bring about an increase in SITH-1-producing cells among OECs. A study finding that job strain was a risk factor for depression (Madsen et al., 2017) is considered to support this hypothesis.

We believe that the present study is the first to demonstrate an influence of a herpesvirus latent protein in a non-oncological disease. Similar to HHV-6B, other non-oncogenic herpesviruses also express (or likely express) latent proteins, so our methods would be applicable to research on the disease risk of other herpesviruses. We consider that our study suggests new directions for research on causes of depression as well as new perspectives for research on this group of viruses and the virome.

Limitations of the Study

When we examined SITH-1 expression in cells infected with HHV-6A and HHV-7, we were unable to detect SITH-1 mRNA with the structure indicated in this study. Additionally, in PCR-based studies (Okuno et al., 1995; Tanaka-Taya et al., 1996; Yoshikawa et al., 2000a, 2000b) and an immunological study (Wang et al., 1999), most Japanese were reported to be infected with HHV-6B. Therefore, we consider our present findings are thought to be limited to HHV-6B. However, if a latent protein with a similar function to SITH-1 can be identified for HHV-6A, it may be possible to extend the results of the present study to HHV-6A.

Resource Availability

Lead Contact

Further information and requests for resources and reagents should be directed to and will be fulfilled by the Lead Contact, Kazuhiro Kondo (kkondo@jikei.ac.jp).

Materials Availability

All unique reagents generated in this study are available from the Lead Contact with a completed Materials Transfer Agreement.

Data and Code Availability

The data included in this manuscript have been deposited in GenBank (accession numbers HV763913.1 and HV763914.1) and Mendeley Data (http://dx.doi.org/10.17632/jxxpc9t732.1).

METHODS

All methods can be found in the accompanying Transparent Methods supplemental file.

SUPPLEMENTAL INFORMATION

Supplemental Information can be found online at https://doi.org/10.1016/j.isci.2020.101187.

ACKNOWLEDGMENTS

We thank Dr. Koichi Yamanishi for his kind advice on this study. We are also grateful to Drs. Hidenori Matsunaga and Osami Kajimoto for clinical assistance and Mr. Alexander Cox for editorial assistance with the manuscript. This work was supported in part by the Ministry of Education, Culture, Sports, Science and Technology (MEXT)-Supported Program for the Strategic Research Foundation at Private Universities (grant number S1201032), Japan; Private University Research Branding Project from MEXT, Japan; grants from the Ministry of Health, Labour and Welfare, Japan; JAPAN TOBACCO Inc.; Virus Ikagaku Kenkyusho Inc.; JSPS KAKENHI Grant Numbers JP23791355, JP26860946, JP25893252, JP16H07220, and JP15K08216, Japan.

AUTHOR CONTRIBUTIONS

N.K., N.O., and K.K. contributed to study design. N.K., N.O., M.T., K.S., A.I., and K.K. contributed to data collection or interpretation. K.K. coordinated all experiments. K.K. identified SITH-1, and N.K., N.O., M.T., K.S., A.I., and K.K. analyzed the function of SITH-1. N.K., N.O., M.T., K.S., Y.T., M.S., H.Y., and K.K. contributed to clinical study and data analysis. N.K., N.O., and K.K. wrote the paper. N.K. and N.O. contributed equally to this work.

DECLARATION OF INTERESTS

K.K. and N.K. have submitted a patent application entitled "Factor involved in latent infection with herpesvirus, and use thereof," US patent application publication 2010/0281550 A1. N.O., K.K., and N.K. have submitted a patent application entitled "Method for detecting antibody against SITH-1 in biological sample," US patent application publication 2012/0107842 A1. K.K. has submitted a patent application entitled "Methods for Assessing Fatigue Level and Applications Thereof," US patent application publication 2008/0280283 A1. K.K. reports grants and non-financial support from Virus Ikagaku Kenkyusho Inc. In addition, K.K. has stock in Virus Ikagaku Kenkyusho Inc.

None of the material has been published or is under consideration by any other journals.

Received: December 8, 2019
Revised: April 20, 2020
Accepted: May 18, 2020
Published: June 26, 2020

REFERENCES

Ablashi, D., Agut, H., Alvarez-Lafuente, R., Clark, D.A., Dewhurst, S., DiLuca, D., Flamand, L., Frenkel, N., Gallo, R., Gompels, U.A., et al. (2014). Classification of HHV-6A and HHV-6B as distinct viruses. Arch. Virol. *159*, 863–870.

Aoki, R., Kobayashi, N., Suzuki, G., Kuratsune, H., Shimada, K., Oka, N., Takahashi, M., Yamadera, W., Iwashita, M., Tokuno, S., et al. (2016). Human herpesvirus 6 and 7 are biomarkers for fatigue, which distinguish between physiological fatigue and pathological fatigue. Biochem. Biophysical Res. Commun. *478*, 424–430.

Belmaker, R.H., and Agam, G. (2008). Major depressive disorder. N. Engl. J. Med. *358*, 55–68.

Conejero-Goldberg, C., Torrey, E.F., and Yolken, R.H. (2003). Herpesviruses and *Toxoplasma gondii* in orbital frontal cortex of psychiatric patients. Schizophr Res. *60*, 65–69.

Major Depressive Disorder Working Group of the Psychiatric GWAS Consortium, Ripke, S., Wray, N.R., Lewis, C.M., Hamilton, S.P., Weissman, M.M., Breen, G., Byrne, E.M., Blackwood, D.H., Boomsma, D.I., et al. (2013). A mega-analysis of genome-wide association studies for major depressive disorder. Mol. Psychiatry *18*, 497–511.

Donati, D., Martinelli, E., Cassiani-Ingoni, R., Ahlqvist, J., Hou, J., Major, E.O., and Jacobson, S. (2005). Variant-specific tropism of human herpesvirus 6 in human astrocytes. J. Virol. *79*, 9439–9448.

Durrant, D.M., Ghosh, S., and Klein, R.S. (2016). The olfactory bulb: an immunosensory effector organ during neurotropic viral infections. ACS Chem. Neurosci. *7*, 464–469.

Harberts, E., Yao, K., Wohler, J.E., Maric, D., Ohayon, J., Henkin, R., and Jacobson, S. (2011). Human herpesvirus-6 entry into the central nervous system through the olfactory pathway. Proc. Natl. Acad. Sci. U S A *108*, 13734–13739.

Hirokawa, T., Boon-Chieng, S., and Mitaku, S. (1998). SOSUI: classification and secondary structure prediction system for membrane proteins. Bioinformatics *14*, 378–379.

Holloway, M.P., and Bram, R.J. (1996). A hydrophobic domain of Ca2+-modulating cyclophilin ligand modulates calcium influx signaling in T lymphocytes. J. Biol. Chem. *271*, 8549–8552.

Jha, H.C., Banerjee, S., and Robertson, E.S. (2016). The role of gammaherpesviruses in cancer pathogenesis. Pathogens *5*.

Keller, J., Gomez, R., Williams, G., Lembke, A., Lazzeroni, L., Murphy, G.M., Jr., and Schatzberg, A.F. (2017). HPA axis in major depression: cortisol, clinical symptomatology and genetic variation predict cognition. Mol. Psychiatry *22*, 527–536.

Kondo, K., Kondo, T., Okuno, T., Takahashi, M., and Yamanishi, K. (1991). Latent human herpesvirus 6 infection of human monocytes/macrophages. J. Gen. Virol. *72*, 1401–1408.

Kondo, K., Sashihara, J., Shimada, K., Takemoto, M., Amo, K., Miyagawa, H., and Yamanishi, K. (2003). Recognition of a novel stage of betaherpesvirus latency in human herpesvirus 6. J. Virol. *77*, 2258–2264.

Kondo, K., Xu, J., and Mocarski, E.S. (1996). Human cytomegalovirus latent gene expression in granulocyte-macrophage progenitors in culture and in seropositive individuals. Proc. Natl. Acad. Sci. U S A *93*, 11137–11142.

Levinson, D.F., Mostafavi, S., Milaneschi, Y., Rivera, M., Ripke, S., Wray, N.R., and Sullivan, P.F. (2014). Genetic studies of major depressive disorder: why are there no genome-wide association study findings and what can we do about it? Biol. Psychiatry *76*, 510–512.

Madsen, I.E.H., Nyberg, S.T., Magnusson Hanson, L.L., Ferrie, J.E., Ahola, K., Alfredsson, L., Batty, G.D., Bjorner, J.B., Borritz, M., Burr, H., et al. (2017). Job strain as a risk factor for clinical depression: systematic review and meta-analysis with additional individual participant data. Psychol. Med. *47*, 1342–1356.

Morales-Medina, J.C., Iannitti, T., Freeman, A., and Caldwell, H.K. (2017). The olfactory bulbectomized rat as a model of depression: the hippocampal pathway. Behav. Brain Res. *317*, 562–575.

Mulligan, S.J., and MacVicar, B.A. (2004). Calcium transients in astrocyte endfeet cause cerebrovascular constrictions. Nature *431*, 195–199.

Negoias, S., Croy, I., Gerber, J., Puschmann, S., Petrowski, K., Joraschky, P., and Hummel, T. (2010). Reduced olfactory bulb volume and olfactory sensitivity in patients with acute major depression. Neuroscience *169*, 415–421.

Okuno, T., Oishi, H., Hayashi, K., Nonogaki, M., Tanaka, K., and Yamanishi, K. (1995). Human herpesviruses 6 and 7 in cervixes of pregnant women. J. Clin. Microbiol. *33*, 1968–1970.

Ota, K.T., Liu, R.J., Voleti, B., Maldonado-Aviles, J.G., Duric, V., Iwata, M., Dutheil, S., Duman, C., Boikess, S., Lewis, D.A., et al. (2014). REDD1 is essential for stress-induced synaptic loss and depressive behavior. Nat. Med. *20*, 531–535.

Otawa, M., Arai, H., and Atomi, Y. (2007). Molecular aspects of adrenal regulation for circadian glucocorticoid synthesis by chronic voluntary exercise. Life Sci. *80*, 725–731.

Pelkmans, L., and de Laat, B. (2012). Antibodies against domain I of beta2-glycoprotein I: the one and only? Lupus *21*, 769–772.

Prusty, B.K., Gulve, N., Govind, S., Krueger, G.R.F., Feichtinger, J., Larcombe, L., Aspinall, R., Ablashi, D.V., and Toro, C.T. (2018). Active HHV-6 infection of cerebellar purkinje cells in mood disorders. Front. Microbiol. *9*, 1955.

Rotola, A., Ravaioli, T., Gonelli, A., Dewhurst, S., Cassai, E., and Di Luca, D. (1998). U94 of human herpesvirus 6 is expressed in latently infected peripheral blood mononuclear cells and blocks viral gene expression in transformed lymphocytes in culture. Proc. Natl. Acad. Sci. U S A *95*, 13911–13916.

Rottstaedt, F., Weidner, K., Strauss, T., Schellong, J., Kitzler, H., Wolff-Stephan, S., Hummel, T., and Croy, I. (2018). Size matters - the olfactory bulb as a marker for depression. J. Affect Disord. *229*, 193–198.

Scharf, S.H., Liebl, C., Binder, E.B., Schmidt, M.V., and Muller, M.B. (2011). Expression and regulation of the Fkbp5 gene in the adult mouse brain. PLoS One *6*, e16883.

Snyder, J.S., Soumier, A., Brewer, M., Pickel, J., and Cameron, H.A. (2011). Adult hippocampal neurogenesis buffers stress responses and depressive behaviour. Nature *476*, 458–461.

Tanaka-Taya, K., Kondo, T., Mukai, T., Miyoshi, H., Yamamoto, Y., Okada, S., and Yamanishi, K. (1996). Seroepidemiological study of human herpesvirus-6 and -7 in children of different ages and detection of these two viruses in throat swabs by polymerase chain reaction. J. Med. Virol. *48*, 88–94.

Thyssen, A., Hirnet, D., Wolburg, H., Schmalzing, G., Deitmer, J.W., and Lohr, C. (2010). Ectopic vesicular neurotransmitter release along sensory axons mediates neurovascular coupling via glial calcium signaling. Proc. Natl. Acad. Sci. U S A *107*, 15258–15263.

Virgin, H.W., and Todd, J.A. (2011). Metagenomics and personalized medicine. Cell *147*, 44–56.

Virgin, H.W., Wherry, E.J., and Ahmed, R. (2009). Redefining chronic viral infection. Cell *138*, 30–50.

Wang, F.Z., Dahl, H., Ljungman, P., and Linde, A. (1999). Lymphoproliferative responses to human herpesvirus-6 variant A and variant B in healthy adults. J. Med. Virol. *57*, 134–139.

Wang, X., Zhang, L., Lei, Y., Liu, X., Zhou, X., Liu, Y., Wang, M., Yang, L., Zhang, L., Fan, S., et al. (2014). Meta-analysis of infectious agents and depression. Sci. Rep. *4*, 4530.

Yamamoto, Y., and Sakisaka, T. (2015). The emerging role of calcium-modulating cyclophilin ligand in posttranslational insertion of tail-anchored proteins into the endoplasmic reticulum membrane. J. Biochem. *157*, 419–429.

Yoshikawa, T., Ihira, M., Suzuki, K., Suga, S., Iida, K., Saito, Y., Asonuma, K., Tanaka, K., and Asano, Y. (2000a). Human herpesvirus 6 infection after living related liver transplantation. J. Med. Virol. *62*, 52–59.

Yoshikawa, T., Ihira, M., Suzuki, K., Suga, S., Matsubara, T., Furukawa, S., and Asano, Y. (2000b). Invasion by human herpesvirus 6 and human herpesvirus 7 of the central nervous system in patients with neurological signs and symptoms. Arch. Dis. Child *83*, 170–171.

iScience, Volume *23*

Supplemental Information

Human Herpesvirus 6B Greatly Increases Risk of Depression by Activating Hypothalamic-Pituitary -Adrenal Axis during Latent Phase of Infection

Nobuyuki Kobayashi, Naomi Oka, Mayumi Takahashi, Kazuya Shimada, Azusa Ishii, Yoshitaka Tatebayashi, Masahiro Shigeta, Hiroyuki Yanagisawa, and Kazuhiro Kondo

Transparent Methods

LEAD CONTACT AND MATERIALS AVAILABILITY

Further information and requests for resources and reagents should be directed to and will be fulfilled by the Lead Contact, Kazuhiro Kondo (kkondo@jikei.ac.jp). All unique reagents generated in this study are available from the Lead Contact with a completed Materials Transfer Agreement.

EXPERIMENTAL MODEL AND SUBJECT DETAILS

Viruses and cells

The macrophage cell lines THP-1 and HL-60 were cultured in Roswell Park Memorial Institute medium (RPMI 1640) containing 10% foetal bovine serum (FBS). The astrocytoma cell lines U373 and A172, as well as HEK293, HEK293T and 3T3 cells, were cultured in Dulbecco's modified Eagle's medium (DMEM) containing 10% FBS. The HST strain of HHV-6B was used to infect the THP-1 and HL-60 cells at a multiplicity of infection (MOI) of 1, and the U373 and A172 cells at an MOI of 10, by centrifugation (37 °C, 2000 × *g*, 30 min). The recombinant adenovirus was produced using an adenovirus expression vector kit (Takara Bio) in accordance with the manufacturer's protocol. A pGfa2Lac plasmid incorporating the GFAP promoter was supplied by Dr. Kazuyoshi Ikuta. The GFAP promoter obtained from the pGfa2Lac plasmid and the SITH-1 gene amplified by PCR were cloned into an adenovirus cosmid vector using standard methods (Ad-GFAP-SITH1). HEK293 cells were transfected with the Ad-GFAP-SITH1 cosmid and a cosmid that did not contain the target gene (pAxcwit). The recombinant adenovirus was prepared in HEK293 cells and purified with an Adeno-X Virus Purification kit (Takara Bio). The purified virus titer was determined using an Adeno-X Rapid Titer kit (Takara Bio).

Sex and age at sampling for the cells were as follows: THP-1, male 1Y; HL-60, female 36Y; U373, male 75Y; A172, male 53Y; HEK293, female fetus; 3T3, male embryo.

Subjects

The study enrolled 84 patients with MDD at the Jikei University Hospital (Tokyo), the Jikei University Kashiwa Hospital (Chiba), Mental Clinic Ogikubo (Tokyo), and Matsushita Hospital (Kagoshima) (44 men, 40 women). They were diagnosed using the structured clinical interview for DSM-IV Axis I disorders, clinician version (SCID-I, CV). A total of 82 volunteers (43 men, 39 women) with no history of psychiatric consultation served as controls. The volunteers were confirmed to have no psychiatric problems using BDI, Chalder Fatigue Scale, SCID-II, Trauma Event Check List, The Center for Epidemiologic Studies Depression Scale (CES-D) as well as through interviews with psychiatrists. Other than stress, factors related to HHV-6B reactivation include drug-induced hypersensitivity syndrome and strong immunosuppression (Table S1). However, the subjects in this

study did not have any symptoms suggestive of these conditions.

To investigate the relationship between stress and HHV-6B in saliva, the study enrolled 110 healthy volunteers (43.6 ± 0.8 [mean ± s.e.m.] years of age; 63 men, 47 women). They were recruited using an advertisement placed by Soiken Inc. Participants were excluded if they were currently taking any chronic medications or supplemental vitamins, or if they weighed less than 40 kg. They were also excluded if they had donated blood within a month of the study, or their blood haemoglobin level was less than 12.0 g/dL.

All human studies were approved by the Ethics Committees of the Jikei University School of Medicine, Tokyo Metropolitan Institute of Medical Science, Soiken Inc., and Soiken Clinic. Written informed consent was obtained from each subject.

Animals

Male 8-week-old C57BL/6NCrSlc mice obtained from Sankyo laboratories were used for all experiments. All mice were housed under standard conditions (12-hour light–dark cycle [lights-on at 8:00 a.m.] at 24 ± 1 °C) with food and water provided ad libitum. All animal experiments were performed in accordance with animal experiment regulations and approved by the Animal Care and Use Committee of the Jikei University School of Medicine.

METHOD DETAILS

Identification of SITH-1 mRNA

We used a previously published HHV-6B latent infection system involving macrophage primary cultures (Kondo et al., 1991). Using the mRNA purified from these primary cultures, a reverse transcription reaction was performed with a random primer, IE4RB, as the reverse transcription primer of the sense transcript, and IE2FB as the reverse transcription primer of the antisense transcript. Next, the product of the reverse transcription (cDNA) was amplified by PCR with the primers IE4RB and IE2FB, and then by double-nested PCR with the inner primers IE4RA and IE2FA.

5′-RACE and 3′-RACE PCR were performed using previously reported methods. Approximately 20 dA residues were added to the 5′ end of the cDNA, to which the anchor primer RL-1 was annealed. For the first 10 cycles of PCR, *Taq* polymerase (Roche Diagnostics) and primers N2 and αR1 were used under the following conditions: thermal denaturation, 94 °C for 1 min; annealing, 55 °C for 1 min; and elongation reaction, 72 °C for 1 min. In subsequent PCR amplification, KOD Plus DNA polymerase (Toyobo) and primers N1 and αR1 were used under the following conditions: thermal denaturation, 94 °C for 1 min; annealing, 65 °C for 30 s; and elongation reaction, 68 °C for 1 min (15 cycles). The PCR amplification products were sequenced.

The anchor primer RL-1 was annealed to the poly-A tail at the cDNA 3′ end. For the first 10 cycles of PCR, *Taq* polymerase (Roche Diagnostics) and primers N2 and αF1 were used under the following conditions: thermal denaturation, 94 °C for 1 min; annealing, 55 °C for 1 min; and elongation reaction, 72 °C for 1 min. In subsequent PCR amplification, KOD Plus DNA polymerase (Toyobo) and primers N1 and αF1 were used under the following conditions: thermal denaturation, 94 °C for 1 min; annealing, 65 °C for 30 s; and elongation reaction, 68 °C for 1 min (15 cycles). The PCR amplification products were sequenced. KEY RESOURCES TABLE lists the primer sequences, and primer positions are indicated in Figure S1.

Yeast two-hybrid screening

The Matchmaker Two-Hybrid System 2 (Clontech Laboratories) was used to screen for proteins that interact with SITH-1 protein following the manufacturer's protocol. SITH-1 was cloned into a pAS2-1 vector to produce a fusion protein of SITH-1 and a GAL4 DNA-binding domain (DNA-BD). SITH-1 was then amplified from SITH-1 cDNA by PCR. To investigate interactions with SITH-1, pAS2-1-SITH-1 was screened against the human foetal brain Matchmaker cDNA Library pACT2 (Clontech Laboratories) and Pretransformed Mouse 17-day Embryo Matchmaker cDNA Libraries (Clontech Laboratories) using a selective culture medium (without histidine, leucine, or tryptophan) in accordance with a standard protocol. Approximately 30 yeast clones were obtained and sequenced, and most were identified to be those including CAML or CAML fragments.

Mammalian two-hybrid assay

A Mammalian Matchmaker Two-Hybrid Assay Kit (Takara Bio) was used to confirm the binding of SITH-1 and CAML in mammalian cells. SITH-1 was cloned into a pM (GAL4) plasmid (pM-SITH-1). Human CAML and mouse CAML were cloned into pVP-16 plasmids (pVP-16-HsCAML, pVP16-MmCAML). Human CAML was amplified by PCR from the human foetal brain Matchmaker cDNA Library pACT2 (Clontech Laboratories). Mouse CAML was amplified by PCR from Mouse 17-day Embryo Matchmaker cDNA Libraries (Clontech Laboratories). HEK293T cells were cotransfected with the pG5SEAP Reporter plasmid; pM-SITH1 or pM (GAL4) plasmid; pVP16-HsCAML, pVP16-MmCAML, or pVP16 plasmid; and the pMetLuc-Control plasmid as an internal control. SEAP activity was measured with the Great EscAPe SEAP Chemiluminescence Kit (Takara Bio). Secreted luciferase activity was measured with the Secreted Luciferase Reporter System (Takara Bio).

Preparation of constitutively SITH-1-expressing U373 cells

A SITH-1-expressing recombinant retrovirus was prepared using the Retro-X Universal Packaging System (Takara Bio) in accordance with standard methods. SITH-1 was cloned into the retrovirus vector pQCXIP (pQC-

SITH-1-IP). This vector can constitutively express the genes for SITH-1, IRES, and puromycin resistance under the control of the cytomegalovirus (CMV) early-stage promoter. The envelope vector p10A1 and either pQC-SITH-1-IP or pQCXIP (no insert) were co-transfected using GP2-293 packaging cells and the calcium phosphate method. The recombinant retrovirus was prepared in the GP2-293 cells, and the viral supernatant was recovered 48 h after transfection. U373-MG astrocytoma cells were infected with the recombinant retrovirus. After infection, the cells were treated with 1 μg/mL puromycin (Calbiochem) to select either constitutively SITH-1-expressing U373 cells (U373-SITH-1) or U373 cells infected with the retrovirus vector (no insert; U373-Vector).

Immunofluorescence staining of cultured cells

Rabbit anti-SITH-1 antibodies were made by inoculating rabbits with GST-tagged SITH-1 protein derived from expression using the pET -42a (+) vector system (Novagen). Stained HHV-6B infected U373 cells were prepared as described in the following. U373 cells were infected (MOI, 10) with HHV-6B using the centrifuge method. At day 1, cells were fixed in cold acetone–methanol for 5 min. The fixed cells were reacted with anti-SITH-1 rabbit polyclonal antibodies combined with OHV-1 or OHV-3 mouse monoclonal antibodies, at 37 °C for 1 h. After washes in PBS, Alexa Fluor 488 goat anti-rabbit secondary antibodies (ThermoFisher) and Alexa Fluor 594 goat anti-mouse secondary antibodies (ThermoFisher) were added, and the mixture reacted at 37 °C for 30 min. The fixed cells were then washed in PBS twice and mounted on slides. The OHV-1 and OHV-3 anti-HHV-6B mouse monoclonal antibodies recognize HHV-6B glycoprotein B and glycoprotein H, respectively, and were kindly provided by Dr. T. Okuno (Hyogo College of Medicine, Nishinomiya, Japan). To stain the U373-SITH-1 and U373-vector cells, they were fixed in cold acetone–methanol for 10 min. The fixed cells were reacted with anti-SITH-1 rabbit polyclonal antibodies and anti-CAML mouse polyclonal antibodies (Abcam) at 37 °C for 1 h. After washes in PBS, Alexa Fluor 594 donkey anti-rabbit secondary antibodies (ThermoFisher) and Alexa Fluor 488 donkey anti-mouse secondary antibodies (ThermoFisher) were added, and the mixture reacted at 37 °C for 30 min. The fixed cells were then washed in PBS twice and mounted on slides. After cover glass application, samples were observed under the same optical conditions using a Carl Zeiss LSM880 confocal microscope equipped with Airyscan (Zeiss, Jena, Germany). The images were acquired by Zen black software (Zeiss).

Measurement of intracellular calcium concentration

U373 cells were first cultured on a glass slide. The fluorescent calcium reagent fura-2 acetoxymethyl ester (fura-2AM, Molecular Probes) was added to DMEM culture medium containing 10% FBS, and reacted at 37 °C for 30 min under dark conditions to allow uptake of the reagent. The cells were washed on the slide and then immersed in Hanks's Balanced Salt Solution with or without calcium. They were then stimulated with the calcium

ATPase inhibitor thapsigargin (100 nM, Calbiochem). Images at excitation wavelengths of 340 nm and 380 nm were taken under a microscope with a CCD camera (IX71, DP70, Olympus) using Lumina Vision software (Mitani Corporation). The mean luminance of six cells was measured in ImageJ (NIH).

Regarding fusion proteins, HEK293T cells or 3T3 cells were cultured on a 96-well plate and transient overexpression of each protein for CAML, SITH-1, N-SITH-CAML-C and N-CAML-SITH-C was achieved for 24 h using Lipofectamine LTX (invitrogen) or Calphos Mammalian Transfection Kit (Clontech). Subsequently, cells were induced to take up Fluo 4-AM using Calcium Kit II-Fluo 4 (Dojindo) and then the fluorescence intensity in individual cells was measured using an ArrayScan XTI instrument (Thermo Fisher) (λex=480nm).

Immunoprecipitation and Immunoblot Analyses

HEK293T cells were transfected with SITH-1 and hCAML/mCAML expression plasmid DNA using the CalPhos Mammalian Transfection Kit. After 24-h incubation, the cells were solubilized with M-PER Mammalian Protein Extraction Reagent. For immunoprecipitation, mouse anti-CAMLG-Ab was immobilized on Dynabeads protein G. As a control, Dynabeads protein G without antibody was used. An equal volume of each cell lysate was incubated with Dynabeads at room temperature for 1 hour using a rotator. The beads were collected and washed with 0.2% Tween20/PBS. The collected beads and cell lysates were analysed by Western blot analysis with rabbit anti-SITH-1-Ab or rabbit anti-CAMLG-Ab.

Nasal inoculation of adenovirus vectors and tissue staining

For the nasal inoculation of adenovirus vectors, 8-week-old male C57BL/6 mice were anaesthetized with isoflurane. Recombinant adenoviruses were diluted in sterile water (not in isotonic buffer). A drop (20 μL) of SITH-Ad or Vector-Ad solution containing the virus at a titer of $1–2 \times 10^9$ plaque-forming units (pfu) /mL was placed at the entrance of the nasal cavity of the mouse. The solution entered the cavity through spontaneous respiration.

For the staining of the olfactory system, mice were sacrificed and transcardially perfused with saline, followed by 10% neutral buffered formalin (pH 7.4). Formalin-fixed tissues were then embedded in paraffin and sectioned. TUNEL staining was performed using the Apoptosis Detection Kit (Takara Bio) in situ. For immunofluorescence staining, paraffin-embedded sections were deparaffinized, and blocking was performed in Image-iT FX Signal Enhancer (Life Technologies) for 30 min. Primary antibodies were obtained from Abcam (active caspase-3 and GFAP) and Takara Bio (NSE). Secondary antibodies were obtained from Thermo (Alexa Fluor 488 Goat Anti-rabbit IgG (H+L), Alexa Fluor 594 Goat Anti-Mouse IgG (H+L)), Donkey anti-Rat IgG (H+L) Secondary Antibody, Alexa Fluor 594). The antibodies were diluted with Can Get Signal Immunostain

Solution A (TOYOBO). After the samples had been mounted on a slide with a cover glass, they were observed under a Keyence BZ-9000 fluorescence microscope.

Oral or intraperitoneal inoculation of adenovirus vectors

A sterile syringe was filled with one hundred μL of SITH-Ad or Vector-Ad solution containing the virus at a titer of 4×10^8 pfu/mL. Depending on the experiment, adenovirus vectors were administered to 8-week-old male C57BL/6 mice by oral gavage or intraperitoneal injection. The mice were bred for a week, examined for depression-like behaviour, and then the olfactory bulb, brain and adrenal glands were harvested.

Intranasal ionomycin administration

Ionomycin (FUJIFILM Wako) was dissolved in methanol to 1 mg/mL, and then diluted 10-fold with saline. Eight-week-old mice were anesthetized, and a total 20 μL volume of 100 μg/mL ionomycin solution was dropped into the nasal cavity of each mouse. The control mice were administered saline containing 10% methanol. These mice were bred for 3 days, and then sacrificed.

Animal behaviour tests

Seven days after the inoculation of SITH-Ad or Vector-Ad, a tail suspension test (TST) (Andreasen et al., 2009) was performed to assess depression-like behaviour. The period of immobility during 10 min was analysed by TailSuspScan software (CleverSys Inc). At 24 h after the TST, the mice were euthanized for real-time PCR and immunohistochemical staining. The antidepressant fluoxetine (FUJIFILM Wako), a selective serotonin reuptake inhibitor (SSRI), was administered via the drinking water (80 mg/L) (Shanahan et al., 2011) 2 weeks before intranasal inoculation.

To examine stress vulnerability, mice were intranasally inoculated with adenovirus vector and kept in a cage with a 20° tilt for 1 week (Harding et al., 2004). The sucrose preference test (Vincent et al., 2013) was used to examine depression-like behaviour. Mice had access to two bottles containing either 1% sucrose or water 3 days before recombinant adenovirus inoculation. After inoculation, each bottle was weighed daily to determine intake. The data are presented as % sucrose intake = sucrose consumed (g) / [water consumed (g) + sucrose consumed (g)].

Real-time PCR

Total RNA was purified from cells using the BioRobot EZ1 and an EZ1 RNA Cell Mini Kit (Qiagen). Total RNA was purified from mouse whole brains using the BioRobot EZ1 and an EZ1 RNA Universal Tissue Kit (Qiagen).

cDNA was synthesized from total RNA with a PrimeScript RT Reagent Kit (Takara Bio). mRNA amounts were quantified in duplicate with FastStart TaqMan Probe Master (Rox) (Roche Diagnostics), and the Applied Biosystems 7300 Real-Time PCR system (Thermo Fisher). The thermal profile was 95 °C for 30 s, followed by 45 cycles of 95 °C for 5 s and 60 °C for 31 s. Data analysis was performed with Sequence Detection Software version 1.4 (Thermo Fisher). SITH-1, U94, H6LT, human GAPDH, mouse BDNF, mouse CRH, and mouse beta-actin (ACTB) were measured using the primers and probes described in Supplementary Table 2.

Antibody titration

To generate the fusion protein expression vectors, SITH-1, a (Gly- Gly- Gly- Gly-Ser) x 5 spacer, and CAML were cloned into pFLAG-CMV-5a (Sigma-Aldrich). pCMV-SITH-1, pCMV- N-SITH-CAML-C, pCMV- N-CAML-SITH-C and pCMV-CAML were transfected into HEK293T cells cultured on Lab-Tek chamber slides (Nunc) using Lipofectamine LTX (Invitrogen). Plasma samples were diluted 1:80 with PBS/2% BSA/0.05% Tween 20, and stained by an indirect immunofluorescence test. The serum was reacted on the slide for 1 h at 37 °C. After washes with PBS/ 0.05% Tween 20, the slide was reacted at 37 °C for 30 min with Alexa Fluor 488 goat anti-human or anti-mouse secondary antibodies (Molecular Probes) diluted 200-fold with PBS/2% BSA/0.05% Tween 20. After washes with PBS/0.05% Tween 20, a cover glass was mounted on the slide. All samples were observed under the same conditions through an Olympus BX51 microscope with a DP-73 CCD camera. The fluorescence intensities of several stained cells in each well were analysed using ImageJ (NIH), and their average was calculated. Antibody titers were indicated as the ratio of [average fluorescence intensity (AFI) of each target antigen minus AFI of untransfected HEK293T cells] to [AFI of pCMV-CAML transfected cells minus AFI of untransfected cells]. The target antigen was HEK293T cells transfected with pCMV-SITH-1, pCMV- N-SITH-CAML-C or pCMV- N-CAML-SITH-C. The Anti-HHV-6B IgG antibody titer was examined using an HHV-6 IgG ELISA Kit (Abnova) in accordance with the manufacturer's recommended protocol.

Quantification of HHV-6B DNA in saliva

Viral DNA was extracted from 400 μL samples of saliva by automatic isolation with the BioRobot EZ1 workstation and EZ1 Virus Mini Kit version 2.0 (Qiagen) in accordance with the manufacturer's protocol. DNA was eluted in 90 μL of elution buffer. Copies of HHV-6B DNA in the saliva samples were quantified by real-time PCR with an Applied Biosystems 7300 Real-Time PCR System. Amplifications were performed in duplicate in a total volume of 50 μL, containing 25 μL of Premix Ex *Taq* (Perfect Real Time; Takara Bio Inc., Otsu, Japan), 0.45 μL of PCR forward primer (100 μM), 0.45 μL of PCR reverse primer (100 μM), 1.25 μL of TaqMan probe (10 μM), 1 μL of Rox reference dye, 5 μL of the viral DNA, and 16.85 μL of PCR-grade water. The thermal

profile was 95 °C for 30 s, followed by 50 cycles of 95 °C for 5 s and 60 °C for 31 s. The primers used for real-time PCR are listed in Supplementary Table 2. Data analysis was performed with Sequence Detection Software version 1.4 (Thermo Fisher).

QUANTIFICATION AND STATISTICAL ANALYSIS

The Shapiro-Wilk normality test was performed to assess the normality of distributions. To compare two different groups, the Mann–Whitney U-test was used as the nonparametric test, and the unpaired *t*-test as the parametric test. To compare multiple groups, one-way analysis of variance (ANOVA) with Fisher's post-hoc test was used as the parametric test and Kruskal-Wallis Test with Steel's post-hoc test as the nonparametric test. Red horizontal lines are means, error bars indicate s.e.m. or median. The χ^2 test was used to test differences between distributions. $P < 0.05$ was considered significant. Spearman rank correlation coefficients were used to determine correlations between variables. Statistical analyses were performed with SPSS Statistics version 19 (IBM) Prism 5 (GraphPad) and BellCurve for Excel (Social Survey Research Information Co., Ltd.).

DATA AND CODE AVAILABILITY

The data included in this manuscript have been deposited in GenBank (accession numbers HV763913.1 and HV763914.1) and Mendeley Data (http://dx.doi.org/10.17632/jxxpc9t732.1).

KEY RESOURCES TABLE

REAGENT or RESOURCE	SOURCE	IDENTIFIER
Antibodies		
Rabbit polyclonal anti-SITH-1	This paper	N/A
anti-CAML goat polyclonal antibodies	Santa Cruz Biotechnology	Cat# sc-7335 RRID: AB_2068676
Rabbit polyclonal anti-Doublecortin	Abcam	Cat# ab18723 RRID:AB_732011
Rat monoclonal anti-BrdU [BU1/75 (ICR1)]	Abcam	Cat# ab6326 RRID: AB_305426
Mouse monoclonal anti-GFAP [GF5]	Abcam	Cat# ab10062 RRID: AB_296804
Rabbit polyclonal anti-active Caspase 3	Abcam	Cat# ab13847 RRID: AB_443014
Mouse monoclonal anti- NSE (3-3-C)	Immuno-Biological Laboratories	Cat# 11031 RRID: AB_494607
Mouse polyclonal anti-CAMLG/CAML	Abcam	Cat# ab67714 RRID: AB_1140196
Rabbit polyclonal anti-CAMLG/CAML	Abcam	Cat# ab236655 RRID: AB_2827929.
Donkey anti-Rabbit IgG (H+L) Highly Cross-Adsorbed Secondary Antibody, Alexa Fluor 594	ThermoFisher	Cat# A-21207 RRID: AB_141637
Goat anti-Mouse IgG (H+L) Cross-Adsorbed Secondary Antibody, Alexa Fluor 594	ThermoFisher	Cat# A-11005 RRID: AB_2534073
Donkey anti-Mouse IgG (H+L) Highly Cross-Adsorbed Secondary Antibody, Alexa Fluor 488	ThermoFisher	Cat# A-21202 RRID: AB_141607
Goat anti-Rabbit IgG (H+L) Highly Cross-Adsorbed Secondary Antibody, Alexa Fluor 488	ThermoFisher	Cat# A-11034 RRID: AB_2576217
Goat polyclonal anti-Human IgG (H+L) Cross-Adsorbed Secondary Antibody, Alexa Fluor 488	ThermoFisher	Cat# A11013 RRID: AB_2534080

Peroxidase-AffiniPure Sheep Anti-Mouse IgG (H+L) (min X Hu,Bov,Hrs Sr Prot) antibody	Jackson ImmunoResearch Labs	Cat# 515-035-062 RRID: AB_2340296
Anti-IgG (H+L chain) (Rabbit) pAb-HRP antibody	MBL International	Cat# 458 RRID: AB_2827722
Bacterial and Virus Strains		
Vector-Ad	TaKaRa Bio	Cat# 6150
SITH-Ad	This paper	N/A
Biological Samples		
human foetal brain Matchmaker cDNA Library pACT2	Clontech Laboratories	Cat# 638869
mouse 17-day-embryo MATCHMAKER cDNA library	Clontech Laboratories	Cat# 638846
Chemicals, Peptides, and Recombinant Proteins		
fura-2 acetoxymethyl ester	ThermoFisher	Cat# F1201
thapsigargin	Merk	Cat# 586005
ionomycin	FUJIFILM Wako Chemicals	Cat# 095-05831
5-Bromo-2′-deoxyuridine	Sigma Aldrich	Cat# B5002
Image-iT FX Signal Enhancer	Invitrogen	Cat# I36933
Can Get Signal Immunostain Solution A	TOYOBO	Cat# NKB-501
fluoxetine	FUJIFILM Wako Chemicals	Cat# 064-04323
Taq DNA Polymerase	Merk	Cat# 11146173001
KOD Plus DNA polymerase	TOYOBO	Cat# KOD-201
Terminal Transferase	New England Biolabs	Cat# M0315S
Premix Ex Taq (Perfect Real Time)	TaKaRa Bio	Cat# RR039A
M-PER Mammalian Protein Extraction Reagent	ThermoFisher	Cat# 78501
Critical Commercial Assays		
Retro-X Universal Packaging System	TaKaRa Bio	Cat# 631530
In situ Apoptosis Detection Kit	TaKaRa Bio	Cat# MK500
CalPhos™ Mammalian Transfection Kit	TaKaRa Bio	Cat# 631312
Calcium Kit II - Fluo 4	Dojindo	Cat# CS32
Lipofectamine LTX Reagent with PLUS Reagent	ThermoFisher	Cat# 15338100

Adeno-X Virus Purification kit	Takara Bio	Cat# 631532
Adeno-X Rapid Titer kit	Takara Bio	Cat# 632250
EZ1 RNA Tissue Mini Kit	QIAGEN	Cat# 959034
EZ1 Virus Mini Kit version 2.0	QIAGEN	Cat# 955134
PrimeScript RT Reagent Kit	Takara Bio	Cat# RR037A
FastStart TaqMan Probe Master (Rox)	Roche Diagnostics	Cat# 04673417001
Matchmaker Two-Hybrid System 2	Clontech Laboratories	Cat# K1604-1
Great EscAPe SEAP Chemiluminescence Kit 2.0	TaKaRa Bio	Cat# 631736
Ready-To-Glow™ Secreted Luciferase Reporter Assay	TaKaRa Bio	Cat# 631726
Retro-X Universal Packaging System	TaKaRa Bio	Cat# 631530
HHV-6 IgG ELISA Kit	Abnova	Cat# KA1457
Dynabeads Protein G Immunoprecipitation Kit	ThermoFisher	Cat# 10007D
Experimental Models: Cell Lines		
Human: THP-1	RIKEN BRC	RCB1189
Human: HL-60	RIKEN BRC	RCB3683
Human: U373 (U-373 MG)	ATCC	HBT-17
Human: A172	RIKEN BRC	RCB2530
Human: HEK293T	RIKEN BRC	RCB2202
Mouse: 3T3 (NIH/3T3)	RIKEN BRC	RCB2767
Experimental Models: Organisms/Strains		
C57BL/6NCrSlc	Japan SLC,Inc.	N/A
Oligonucleotides		
αF1 primer CTGAAGCATGTAAGCACATCTCTTGC	This paper	N/A
αR1 primer GCTTCGAGATCAGTAGTGGTACG	This paper	N/A
IE2FA primer GAAACCACCACCTGGAATCAATCTCC	This paper	N/A
IE2FB primer CATCCCATCAATTATTGGATTGCTGG	This paper	N/A

IE4RA primer GACACATTCTTGGAAGCGATGTCG	This paper	N/A
IE4RB primer GATGCTCCTTCTTCCACATTACTGG	This paper	N/A
N1 primer GCTGGGTAGTCCCCACCTTTCTAGA	This paper	N/A
N2 primer CTTATGAGTATTTCTTCCAGGGTACTCGAG	This paper	N/A
RL-1 primer CTTATGAGTATTTCTTCCAGGGTACTCGAGGCTGGG TAGTCCCCACCTTTCTAGATTTTTTTTTTTTTTTTT	This paper	N/A
SITH-1 qPCR F: CCAGCTGCACTGAATCCAC R: GCCTGAACCCAACTTGGAG P: FAM- CTTCTGTACATACCGATTCTGTGACGAGCC -TAMRA	This paper	N/A
H6S qPCR F: TCCGGAGAACATTCTCATCACA R: GTGGAGGTTTCTTTGGAGATTGA P: FAM- TCGGGTGCAATCAATCTTTCTTCTGGGC -TAMRA	This paper	N/A
Hs_GAPDH qPCR F: CACCATGGGGAAGGTGAAGG R: CAATATCCACTTTACCAGAGTTAAAAGC P: FAM- CGCCCAATACGACCAAATCCGTTGACTCC -TAMRA	This paper	N/A
Mm_Bax qPCR F: ACTGGACTTCCTCCGTGAGC R: GGGGTCCCGAAGTAGGAGAG P: FAM-CCTTCCCAGCCACCCTGGTCTTGGAT-TAMRA	This paper	N/A

Mm_Bcl-2 qPCR F: CTCAGCCCTGTGCCACCTG R: ACTGGACATCTCTGCGAAGTCA P: FAM-AGCGACGAGAGAAGTCATCCCCAGCC-TAMRA	This paper	N/A
Mm_ACTB qPCR F: CGCGAGCACAGCTTCTTTG R: CGACCAGCGCAGCGATATC P: FAM- CACACCCGCCACCAGTTCGCCATG -TAMRA	This paper	N/A
Mm_CRH qPCR F: TCCGCATGGGTGAAGAATACTTC R: TGAGGGGCGTGGAGTTGG P: FAM-CAACAGAAGTCCCGCTGCTCGGCTG-TAMRA	This paper	N/A
Mm_FKBP5 qPCR F: GCGGGACGCAAAGGAGGA R: CATGGCCTGACTCTCGTGTTG P: FAM-CTCCTTCTACAGCCTTCTTGCTCCCAGC-TAMRA	This paper	N/A
Mm_REDD1 qPCR F: CGGGCCGGAGGAAGACTC R: CTGCATCAGGTTGGCACACA P: FAM-TCATCCTCGGGGTCACTGAGCAGCTC-TAMRA	This paper	N/A
Mm_StAR qPCR F: GAGTGGTGTCATCAGAGCTGAA R: TGCGATAGGACCTGGTTGATG P: FAM- TTGTCTTCGGCAGCCACCCCTTCAG -TAMRA	This paper	N/A

Mm_IL-1β qPCR F: CCTGAACTCAACTGTGAAATGCC R: CTGCTGCGAGATTTGAAGCTG P: FAM-TGCTCTCATCAGGACAGCCCAGGTCA-TAMRA	This paper	N/A
Mm_IL-6 qPCR F: CCGGAGAGGAGACTTCACAGA R: GTTGTTCATACAATCAGAATTGCCATT P: FAM-ACCACTCCCAACAGACCTGTCTATACCACT-TAMRA	This paper	N/A
Mm_TNF-α qPCR F: CCAGACCCTCACACTCAGATCAT R: CCTCCACTTGGTGGTTTGCTAC P: FAM- ATTCGAGTGACAAGCCTGTAGCCCACG -TAMRA	This paper	N/A
Mm_IL-10 qPCR F: CTGAGGCGCTGTCATCGA R: ACACCTTGGTCTTGGAGCTTAT P: FAM- AATCACTCTTCACCTGCTCCACTGCCT -TAMRA	This paper	N/A
Mm_ IL-1rn qPCR F: TGCCGCCCTTCTGGGAAA R: CTGGTTGTTTCTCAGGTAAAAGGTC P: FAM- CCCAGATTCTGAAGGCTTGCATCTTGCA -TAMRA	This paper	N/A
Mm_OAS1a/g qPCR F: CGTCAATGTCGTGTGTGATTTCC R: TTGAGTGTGGTGCCTTTGCC P: FAM- AGAGATGCTTCCAAGGTGCTGCCCA -TAMRA	This paper	N/A

Mm_IFNA2 qPCR F: CTGTGCTTTCCTCGTGATGC R: CTCATCTGTGCCAGGACCTTC P: FAM- ACCTGTTCTCTAGGATGCGATCTGCCTC -TAMRA	This paper	N/A
Mm_IFNA4 qPCR F: TGCTTTCCTCATGATCCTGGTAAT R: CTTCTCATTTCTTCCAGGACTGTC P: FAM- TGAGCTACTACTGGTCAGCCTGTTCTCT -TAMRA	This paper	N/A
Mm_ IFNA5 qPCR F: AGAAAGGACTTTGGATTCCCACA R: CTGGGTCAGCTCACTCAGGA P: FAM- TGGATCTGCTGGGCACCCACCTTC -TAMRA	This paper	N/A
Mm_ IFNB1 qPCR F: ACTAGAGGAAAAGCAAGAGGAAAGA R: GTACCTTTGCACCCTCCAGTAAT P: FAM- AGAGCAGTTGAGGACATCTCCCACGTC -TAMRA	This paper	N/A
HHV-6B qPCR F: GACAATCACATGCCTGGATAATG R: TGTAAGCGTGTGGTAATGGACTAA P: FAM- AGCAGCTGGCGAAAAGTGCTGTGC -TAMRA	This paper	N/A

HHV-6_U94 qPCR F: GAGCGCCCGATATTAAATGGAT R: GCTTGAGCGTACCACTTTGCA P: FAM- CTGGAATAATAAAACTGCCGTCCCCACC - TAMRA	Caruso, A., Caselli, E., Fiorentini, S., Rotola, A., Prandini, A., Garrafa, E., Saba, E., Alessandri, G., Cassai, E., and Di Luca, D. (2009). U94 of human herpesvirus 6 inhibits in vitro angiogenesis and lymphangiogenesis. Proc Natl Acad Sci U S A 106, 20446-20451.	N/A
H6LT F: GTCGTTCTTAATTCACTGAGTTCTG R: GTGGAGGTTTCTTTGGAGATTGA P: FAM- TCGGGTGCAATCAATCTTTCTTCTGGGC - TAMRA	This paper	N/A
Recombinant DNA		
pM-SITH-1	This paper	N/A
pVP-16-HsCAML	This paper	N/A
pVP16-MmCAML	This paper	N/A
pFlag-CMV-5b	Sigma Aldrich	Cat# E3762
SITH-1/pFlag-CMV-5b	This paper	N/A
CAML/pFlag-CMV-5b	This paper	N/A
N-SITH-CAML-C/pFlag-CMV-5b	This paper	N/A
N-CAML-SITH-C/pFlag-CMV-5b	This paper	N/A
Software and Algorithms		
Lumina Vision software	Mitani Corporation	https://www.mitani-visual.jp/products/bio_imaging_analysis/lumina_vision/

ImageJ	NIH	https://imagej.nih.gov/ij/
Sequence Detection Software version 1.4	Thermo Fisher	N/A
SPSS Statistics	IBM	https://www.ibm.com/jp-ja/products/spss-statistics
Prism 5	GraphPad	N/A
BellCurve for Excel	Social Survey Research Information Co., Ltd	https://bellcurve.jp/ex/
TailSuspScan	CleverSys Inc	N/A
ArrayScan XTI instrument	Thermo Fisher	N/A
ACTIMO-DATA	Nihon Bioresearch Inc	N/A
Image Lab	Bio-Rad Laboratories	Cat# 1709690
Zen black software	Zeiss	N/A

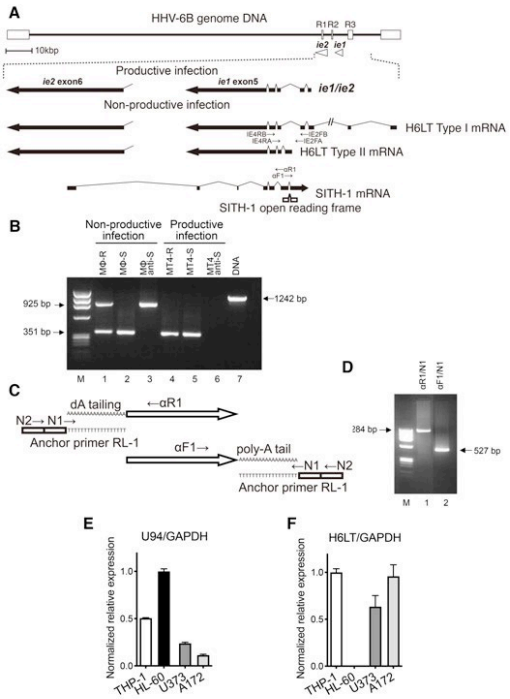

Figure S1 Identification of HHV-6B latent gene encoding SITH-1 (small protein encoded by the intermediate stage transcript of HHV-6-1), Related to Figure 1.

(A) Primer design for PCR-based SITH-1 cloning, and structure obtained for SITH-1. Upper portion, structure of HHV-6B, including repeat sequences; middle portion, structure of HHV-6B latent transcript H6LTs; bottom portion, structure of newly identified antisense latent transcript and encoded protein SITH-1. Fine lines, introns; thick arrows, exons; fine arrows, primers used in double-nested PCR and RACE.

(B) Amplification of latent transcripts. The mRNA obtained from latently infected cells was amplified by double-nested RT-PCR (lanes 1–3). MT-4 cells productively infected with HHV-6B were used as controls (lanes 4–6). At the time of reverse transcription, a random primer (lanes 1, 4: MΦ-R, MT4-R), IE4RB (lanes 2, 5: MΦ-S, MT4-S), or IE2FB (lanes 3, 6: MΦ anti-S, MT4 anti-S) was used. The cDNAs (lanes 1–6) and HHV-6B DNA (lane 7) were amplified with double-nested PCR using the outer primers IE4RB-IE2FB and the inner primers IE4RA-IE2FA.

(C) 3′ - and 5′ -RACE primers to determine structure of mRNA from latency-associated gene.

(D) Electrophoresis of products amplified using 5′ -RACE and 3′ -RACE. Lane 1, 5′ -RACE products; lane 2, 3′ -RACE products; M, size markers.

(E, F) Expression of U94 mRNA (E) and H6LT mRNA (F) in macrophage (MΦ) cell lines (THP-1 and HL-60) and astrocyte cell lines (U373 and A172). Ratios of SITH-1 to glyceraldehyde-3-phosphate dehydrogenase (GAPDH) are shown.

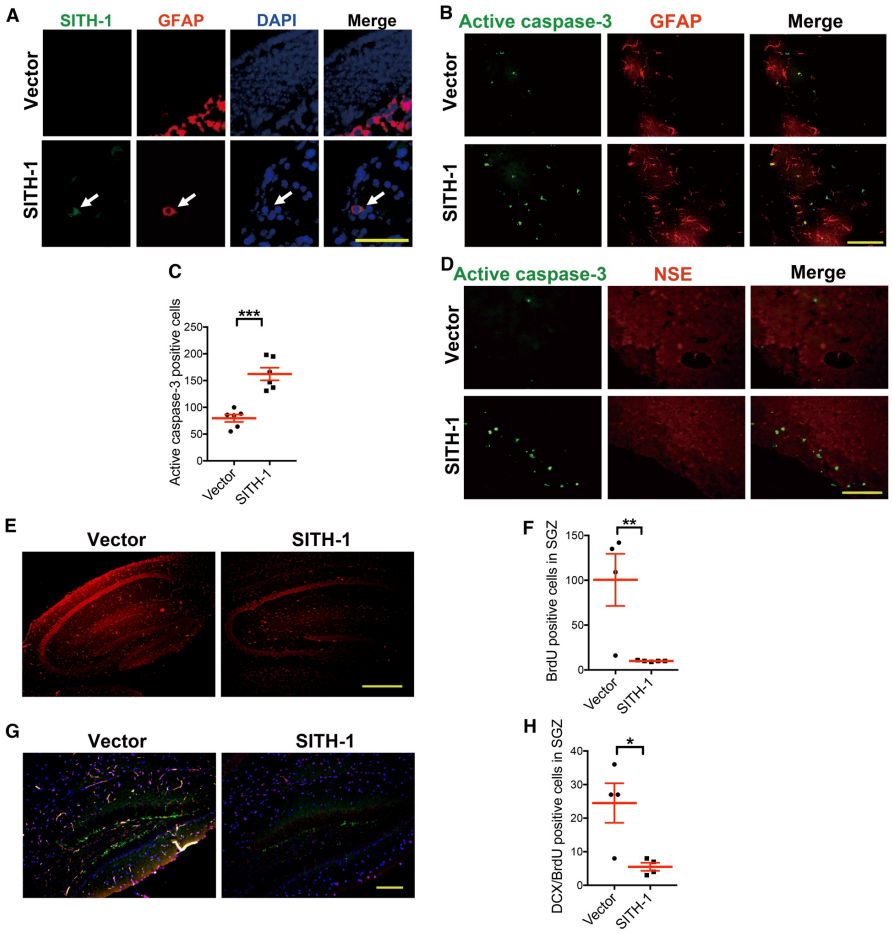

Figure S2 Characterization of SITH-1 expressing mice, Related to Figures 1 and 2.

Mice were inoculated intranasally with empty adenovirus (vector) or SITH-1 adenovirus (SITH-1).

(A) SITH-1 expression in olfactory astrocytes. Green, SITH-1; red, GFAP; blue, DAPI. Scale bar: 50 μm.

(B) Detection of active caspase 3-positive apoptotic cells in OB. Sagittal sections of OB were stained using anti-activated caspase 3. Green, activated caspase 3; red, GFAP.

(C) Numbers of caspase 3-positive cells in each section. Values are means ± s.e.m. Unpaired t-test; ***, P<0.001.

(D) No increase in caspase 3 positive cells in NSE positive neurons was observed. Green, activated caspase 3; red, neuron-specific enolase (NSE). Scale bars, 100 μm (B, D).

(E) BrdU staining of hippocampal dentate gyrus (DG). Red, BrdU. Scale bar: 300 μm.

(F) Numbers of BrdU-positive cells in subgranular zone (SGZ) in each section.

(G) Double staining of hippocampal dentate gyrus with DCX and BrdU. Green, DCX; red, BrdU; blue, DAPI. Scale bar: 100 μm.

(H) Numbers of DCX/BrdU-positive cells in SGZ in each section.

F, H: Values are means ± s.e.m. Unpaired t-test; *, P<0.05; **, P<0.01.

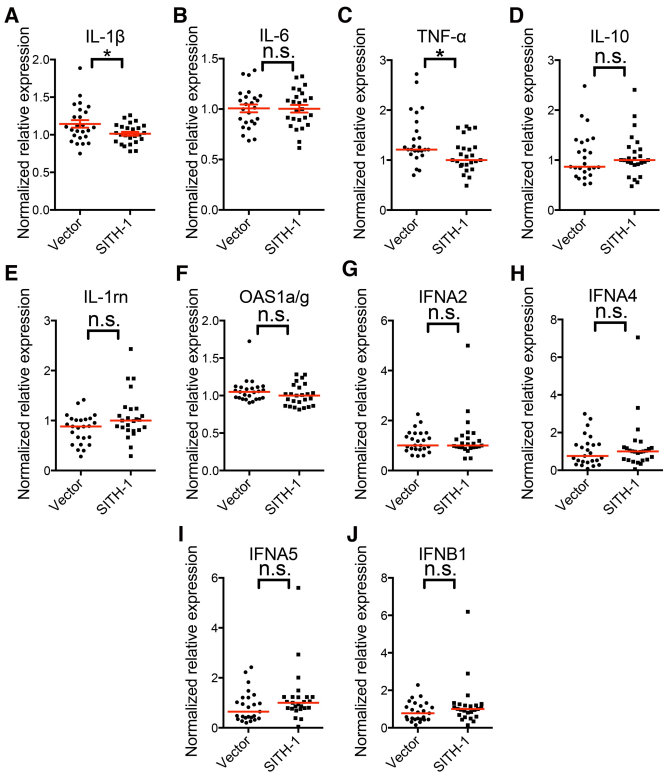

Figure S3 Inflammatory cytokines, interferons, and related factors in SITH-1 mouse brain and olfactory bulb (OB), Related to Figure 2.

Expression of indicated mRNAs at 1 week postinoculation (p.i.) in whole mouse brains excluding the OB (A-F) and OB (G-J). Ratios to beta-actin (ACTB) are shown.

IL, interleukin; TNF, tumor necrosis factor; IL-1rn, interleukin 1 receptor antagonist; OAS1a/g, 2′ -5′ oligoadenylate synthetase; IFNA, interferon alpha; IFNB, interferon beta.

A, B: Values are means ± s.e.m. Unpaired t-test; *, $P<0.05$; n.s., not significant.

C-J: Bars represent median values; Mann–Whitney U-test. *, $P<0.05$; n.s., not significant.

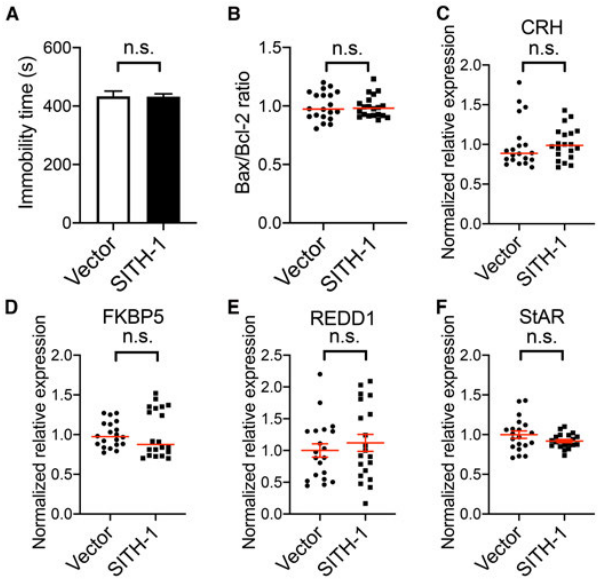

Figure S4 Behavior of mice and gene expression after oral administration of SITH-1 adenovirus, Related to Figure 2.

(A) Prolonged immobility in TST.

(B) Olfactory bulb apoptosis (Bax/Bcl-2 ratio).

(C-F) Expression of indicated mRNAs related to HPA axis activation.

A, E, F: Values are means ± s.e.m. Unpaired t-test; n.s., not significant.

B, C, D: Bars represent median values; Mann–Whitney U-test. n.s., not significant.

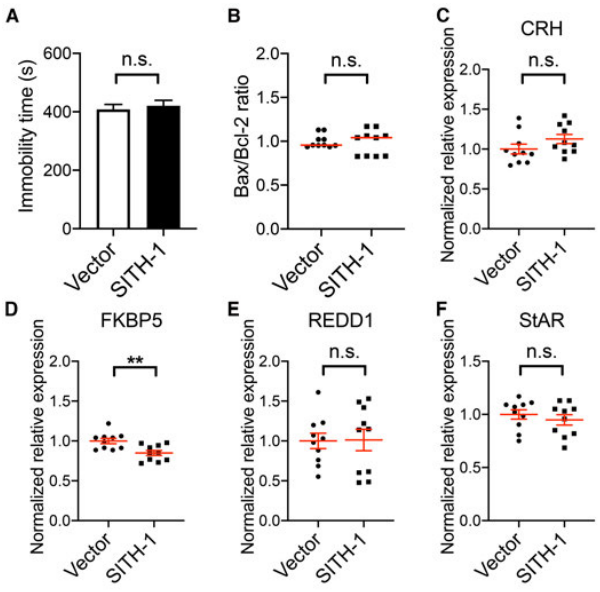

Figure S5 Behavior of mice and gene expression after intraperitoneal inoculation with SITH-1 adenovirus, Related to Figure 2.

(A) Prolonged immobility in TST.

(B) Olfactory bulb apoptosis (Bax/Bcl-2 ratio).

(C-F) Expression of indicated mRNAs related to HPA axis activation.

A, E, F: Values are means ± s.e.m. Unpaired t-test; n.s., not significant.

B, C, D: Bars represent median values; Mann–Whitney U-test. n.s., not significant.

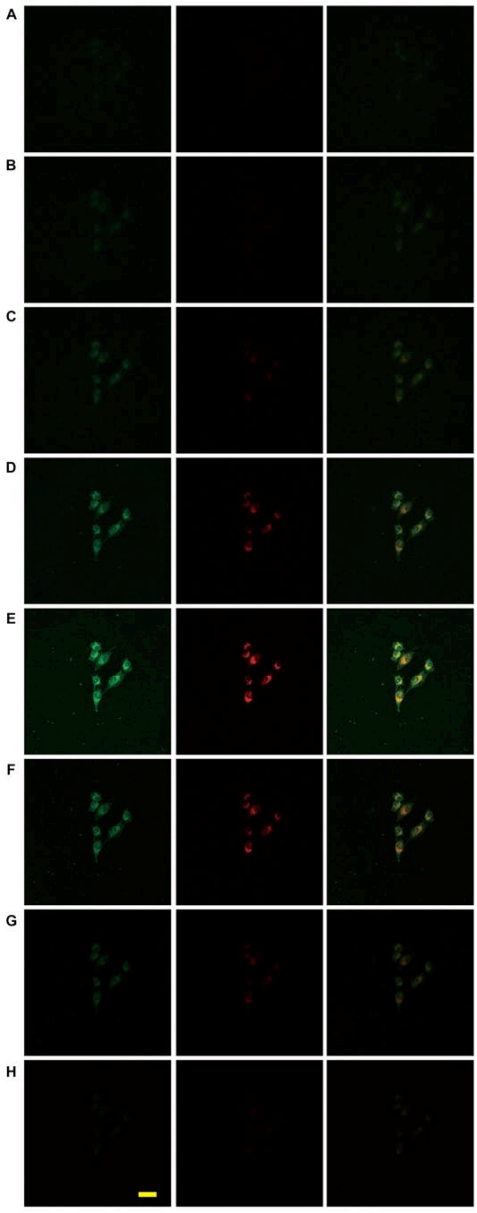

Figure S6 Z-stack images of SITH-1 expressing U373 cells, Related to Figure 3.

Colocalization of SITH-1 and CAML in astrocytes. U373 cells expressing SITH-1 were immunostained. Z-stack images are shown. Z-stacks were acquired using confocal microscopy. Samples were vertically scanned from the bottom of the coverslip with a 20 x objective.

(A) Upper images of cells.

(B-H) Each subsequent image was taken 2.287μm deeper than previous one.

Red, SITH-1; green, CAML. Merge, merged image of the SITH-1 and CAML staining. Bar, 50μm.

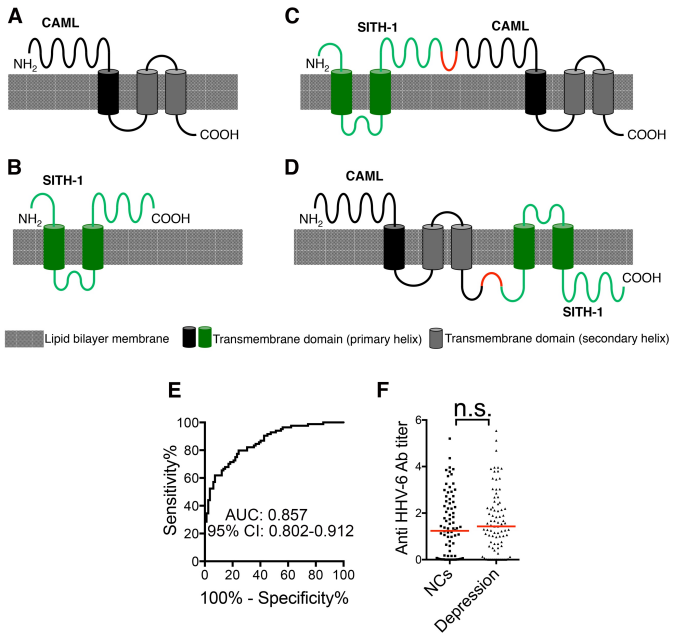

Figure S7 Evidence for SITH-1 expression in depressive patients, Related to Figure 4.

Shows results of secondary structural analysis of CAML (A), SITH-1 (B), N-SITH-CAML-C (C) and N-CAML-SITH-C (D) using SOSUI. Transmembrane regions are shown as cylinders. Black cylinders are CAML, green cylinders are SITH-1 and red lines indicate spacers.

(E) ROC curve for anti-N-SITH-CAML-C antibody titers and depression diagnosis. Area under ROC curve: 0.8573. P<0.0001. Total number of subjects in study: 166, true positive: 67, true negative: 62.

(F) Anti-HHV-6 antibody titers in depressive patients and NCs. Bars represent median values. Mann–Whitney U-test; n.s., not significant.

Table S1. Subject characteristics, Related to Figure 4.

	Control (n = 82)	MDD (n = 84)	P
Age, mean (s.e.m.) years	45.1 (1.7)	48.7 (1.5)	n.s.
Sex, n (%) men	43 (52.4)	44 (52.4)	n.s.
Age at onset, mean (s.e.m.) years		41.7 (1.5)	
BDI, mean (s.e.m.)	2.7 (0.3)	18.3 (1.6)[a]	< 0.0001

[a] n = 80